Density-Softmax: Efficient Test-time Model for Uncertainty Estimation and Robustness under Distribution Shifts

Ha Manh Bui [1] **Anqi Liu** [1]

Abstract

Sampling-based methods, e.g., Deep Ensembles and Bayesian Neural Nets have become promising approaches to improve the quality of uncertainty estimation and robust generalization. However, they suffer from a large model size and high latency at test time, which limits the scalability needed for low-resource devices and real-time applications. To resolve these computational issues, we propose Density-Softmax, a sampling-free deterministic framework via combining a density function built on a Lipschitz-constrained feature extractor with the softmax layer. Theoretically, we show that our model is the solution of minimax uncertainty risk and is distance-aware on feature space, thus reducing the over-confidence of the standard softmax under distribution shifts. Empirically, our method enjoys competitive results with state-of-the-art techniques in terms of uncertainty and robustness, while having a lower number of model parameters and a lower latency at test time.

1. Introduction

The ability of models to produce high-quality uncertainty estimation and robustness is crucial for reliable Deep Neural Network (DNN) in high-stake applications (e.g., healthcare, finance, decision-making, etc.). In principle, a **reliable model** permits graceful failure, signaling when it is likely to be wrong (**uncertainty**), and also generalizes better under distribution shifts (**robustness**) (Tran et al., 2022). Additionally, to be widely used in real-world scenarios, the reliable DNN model also necessarily needs to be fast and lightweight (**efficiency**). This efficiency criterion can be considered in two phases, training time and test time. At **training time**, an inefficient DNN model might be acceptable given the high computational resources in development. However, at **test time**, inefficiency is a critical issue for users when the model needs to be deployed on low-resource devices and in real-time applications (Hinton et al., 2015).

Method	Uncertainty quality	Robustness quality	Test-time efficiency	Without prior requirement
Deterministic	✗	✗	✓	✓
Bayesian	✓	✗	✓	✗
Ensembles	✓	✓	✗	✓
Ours	✓	✓	✓	✓

Table 1. A comparison between methods regarding uncertainty, robustness quality, test-time efficiency (lightweight & fast), and whether pre-defined prior hyper-parameters are required.

Deterministic Empirical Risk Minimization (ERM) (Vapnik, 1998) model nowadays can be efficient due to being **sampling-free** with $\mathcal{O}(1)$ sample complexity, i.e., it only needs a single forward pass with a single DNN model to produce the softmax probability. However, it often struggles with over-confidence and over-fitting. This poor performance usually occurs when the test data is far and does not come from the same distribution as the training set (Minderer et al., 2021; Bui et al., 2021; Bui & Maifeld-Carucci, 2022; Ovadia et al., 2019; Guo et al., 2017).

To improve uncertainty estimation and robustness under distribution shifts, recent **sampling-based** approaches with $\mathcal{O}(M)$ sample complexity, where M is the number of sampling times, have shown promising results (Collier et al., 2021; Dusenberry et al., 2020; Wen et al., 2020). Among these works, the best performance in practice so far is based on Deep Ensembles (Lakshminarayanan et al., 2017; Tran et al., 2022; Nado et al., 2021). However, this approach suffers from a heavy computational burden as it requires more model parameters and multiple forward passes, leading to inefficiency at test time. To tackle this challenge, sampling-free methods (Mukhoti et al., 2023; Charpentier et al., 2022; Liu et al., 2020a; Havasi et al., 2021), and lightweight sampling-based models (Wen et al., 2020; Dusenberry et al., 2020) have been recently proposed. Nevertheless, besides generally performing worse than Deep Ensembles, these methods are also less computationally efficient than Deterministic ERM (Nado et al., 2021) (e.g., Tab. 1).

[1]Department of Computer Science, Johns Hopkins University, Baltimore, MD, U.S.A. Correspondence to: Ha Manh Bui <hb.buimanhha@gmail.com>.

Proceedings of the 41st International Conference on Machine Learning, Vienna, Austria. PMLR 235, 2024.

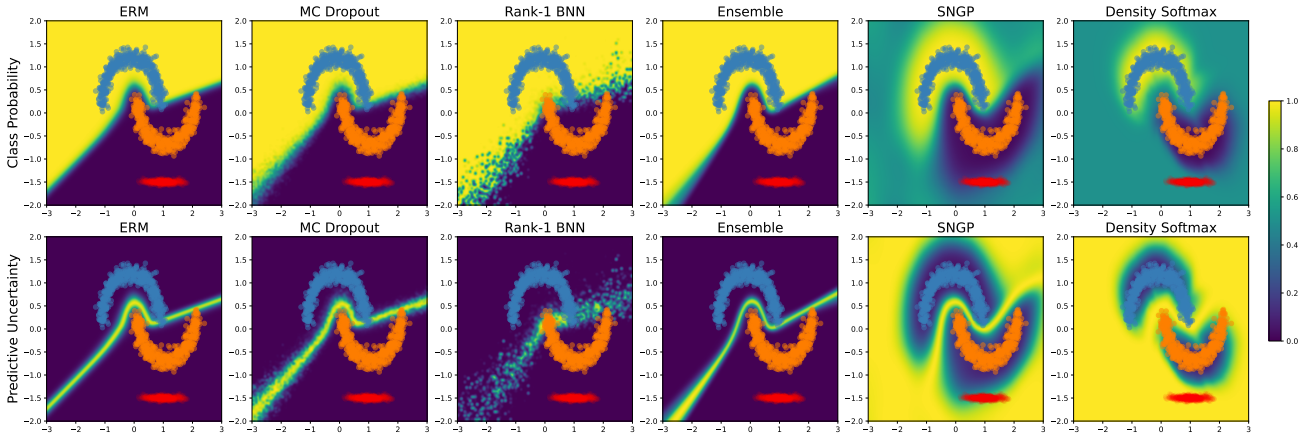

Figure 1. The class probability $p(y|x)$ (Top Row) and predictive uncertainty $var(y|x) = p(y|x) \cdot (1 - p(y|x))$ surface (Bottom Row) as background colors in a comparison between our Density-Softmax and different approaches on the two moons 2D classification. Training data for positive (Orange) and negative classes (Blue) are shown. OOD data (Red) are not observed during training. **Our Density-Softmax achieves distance awareness with a uniform class probability and high uncertainty value on OOD data**. A quick demo is available at https://colab.research.google.com/drive/1dqaacHzOHUPFhBDcUw7yGL-zv7GSG-8P?usp=sharing.

Toward a model that keeps the Deep Ensembles performance with test-time efficiency similar to Deterministic ERM, we introduce Density-Softmax, a sampling-free single-model via a combination of a density function and a Lipschitz-constrained feature extractor. By using regularization to enforce the 1-Lipschitz constraint in training, our model can improve the robustness under distribution shifts. In addition, by combining the feature density function with the softmax layer via a single forward pass, our method only needs a small number of additional parameters and latency when compared to Deterministic ERM. Importantly, this combination helps Density-Softmax be feature distance aware, i.e., its associated uncertainty metrics are monotonic functions of feature distance metrics, leading to a good uncertainty notion of when the test feature is near or far from the training set. This distance-aware property is important to help DNN for both calibration and OOD detection, however, it is often not guaranteed for typical DNN models (Liu et al., 2020a; Manh Bui & Liu, 2024) (e.g., Fig. 1).

To summarize, our model includes three main components: a Lipschitz-constrained feature extractor, a lightweight Normalizing-Flows density model on the feature space, and a classifier with the softmax layer. In training time, the feature extractor is pre-trained using ERM objective and gradient-penalty regularization, aiming to achieve the 1-Lipschitz constraint. After that, the Normalizing-Flows model estimates a marginal density of the learned low-dimensional feature space. Finally, the classifier is fine-tuned with feature likelihood from the density model. In test time, the feature likelihood is combined directly with the logit vector of the classifier to produce a softmax probability with only a single forward pass.

Our contributions can be summarized as follows:

1. We introduce Density-Softmax, a reliable, sampling-free, and single DNN framework via a direct combination of a density function built on a Lipschitz-constrained feature extractor with the softmax layer. Notably, our algorithm does not require any data augmentation (Hendrycks* et al., 2020; Zhang et al., 2018), the OOD set, or the post-hoc re-calibration technique (Mukhoti et al., 2023) in training.

2. We formally prove that our model is the solution to the minimax uncertainty risk, its distance awareness on the feature space, and can reduce over-confidence of the standard softmax when the test feature is far from the training set.

3. We empirically show that our framework achieves a competitive robust generalization and uncertainty estimation performance with SOTA on the Toy dataset with ResFFN-12-128, shifted CIFAR-10-100 with Wide Resnet-28-10, and ImageNet with ResNet-50. Importantly, Density-Softmax requires only a single forward pass and a lightweight feature density function. Therefore it has fewer parameters and is much faster than other baselines at test time.

2. Related work

Uncertainty and Robustness. Nado et al. (2021); Bui & Maifeld-Carucci (2022) has studied the uncertainty and robustness of modern DNN approaches extensively in the benchmark of SOTA baselines, mainly evaluating NLL, in-out accuracy for robust generalization, and ECE for cal-

ibrated uncertainty. More modern discussion of reliable DNN can be found in the literature of Tran et al. (2022). Among these methods, sampling-based approaches are widely used, from Gaussian Process (Gardner et al., 2018; Lee et al., 2018a), Dropout (Gal & Ghahramani, 2016a; Gal et al., 2017), BNN (Blundell et al., 2015; Wen et al., 2018; Maddox et al., 2019), to the SOTA Ensembles (Lakshminarayanan et al., 2017). However, these methods often have a high number of model parameters. To resolve this issue, lightweight sampling-based models, e.g., BatchEnsemble (Wen et al., 2020), Rank-1 BNN (Dusenberry et al., 2020), and Heteroscedastic (Collier et al., 2021) have been proposed recently.

Sampling-free methods. To tackle the scalability challenge in sampling-based methods, novel sampling-free methods have been investigated, including replacing the loss function (Wei et al., 2022; Malinin & Gales, 2018; 2019; Kotelevskii et al., 2022; Karandikar et al., 2021), the output layer (Manh Bui & Liu, 2024; Van Amersfoort et al., 2020; Mukhoti et al., 2023; Tagasovska & Lopez-Paz, 2019; Wang et al., 2022; Liu et al., 2020b), or computing a closed-form posterior in Bayesian inference (Kopetzki et al., 2021; Sensoy et al., 2018; Riquelme et al., 2018; Snoek et al., 2015; Kristiadi et al., 2020; Charpentier et al., 2022). Nevertheless, these methods often only focus on improving uncertainty quality without improving accuracy or even using additional re-calibration set to enhance this performance (Mukhoti et al., 2023). In the scope of uncertainty and robustness (Nado et al., 2021), there exist distillation approaches (Vadera et al., 2020; Malinin et al., 2020) and closest to our work is MIMO (Havasi et al., 2021), Posterior Net (Charpentier et al., 2020), and SNGP (Liu et al., 2020a). Although these methods can improve efficiency at test time, they still underperform Deep Ensembles regarding reliability and Deterministic ERM regarding the model's test-time efficiency.

Improving uncertainty quality via density estimation. Enhancing uncertainty estimates via density function has shown promising results in practice (Manh Bui & Liu, 2024; Kuleshov & Deshpande, 2022; Charpentier et al., 2020; Mukhoti et al., 2023; Kotelevskii et al., 2022; Dosovitskiy et al., 2021; Lee et al., 2018b; Sun et al., 2022). That said, Dosovitskiy et al. (2021); Lee et al. (2018b); Sun et al. (2022) suffer from a heavy computational burden at test time and only focus on OOD detection. Meanwhile, our efficient method additionally provides both empirical and theoretical analysis of the calibration level (details are in Apd. B.4). Theoretically, Charpentier et al. (2022) proves with a small number of parameters, the Normalizing-Flows model can improve the uncertainty notion of DNN by providing a high likelihood when the test feature is close and a low likelihood when that is far from training data. However, this work customizes the last layer of DNN with sensitive priors, not normalized by a natural exponent function, resulting in a bad robustness performance (Nado et al., 2021). In our work, Density-Softmax utilizes a Normalizing-Flows model on the Lipschitz-constrained feature together with the logit vector of the classifier to improve the robust accuracy, uncertainty quality, and test-time efficiency.

Improving robustness via 1-Lipschitz constraint. 1-Lipschitz Neural Nets have been widely used to train certifiably robust classifiers in practice (Tsuzuku et al., 2018; Béthune et al., 2022; Li et al., 2019; Searcód, 2006). It is theoretically shown to be able to defend against adversarial attack (Li et al., 2019), preserve accuracy on IID, and improve the robust generalization on OOD data (Béthune et al., 2022). However, it is not clear whether this property can contribute to better uncertainty estimation. In this work, we integrate the Lipschitz-constrained feature extractor from gradient-penalty regularization (Gulrajani et al., 2017) with our density estimation component to achieve better robust accuracy, uncertainty quality, and test-time efficiency.

3. Density-Softmax

3.1. Notation and Problem setting

Let $\mathcal{X}$ and $\mathcal{Y}$ be the sample and label space. Denote the set of joint probability distributions on $\mathcal{X} \times \mathcal{Y}$ by $\mathcal{P}_{\mathcal{X}\times\mathcal{Y}}$. A dataset is defined by a joint distribution $\mathbb{P}(X, Y) \in \mathcal{P}_{\mathcal{X}\times\mathcal{Y}}$, and let $\mathcal{P}$ be a measure on $\mathcal{P}_{\mathcal{X}\times\mathcal{Y}}$, i.e., whose realizations are distributions on $\mathcal{X} \times \mathcal{Y}$. Denote the training set by $D_s = \{(x_s^i, y_s^i)\}_{i=1}^{n_s}$, where n_s is the number of data points in D_s, s.t., $(x_s, y_s) \sim \mathbb{P}_s(X, Y)$ and $\mathbb{P}_s(X, Y) \sim \mathcal{P}$. In the standard learning setting, a learning model that is only trained on D_s, arrives at a good generalization performance on the test set $D_t = \{(x_t^i, y_t^i)\}_{i=1}^{n_t}$, where n_t is the number of data points in D_t, s.t., $(x_t, y_t) \sim \mathbb{P}_t(X, Y)$ and $\mathbb{P}_t(X, Y) \sim \mathcal{P}$. In the Independent-identically-distributed (IID) setting, $\mathbb{P}_t(X, Y)$ is similar to $\mathbb{P}_s(X, Y)$, and let us use $\mathbb{P}_{iid}(X, Y)$ to represent the IID test distribution. In contrast, $\mathbb{P}_t(X, Y)$ is different with $\mathbb{P}_s(X, Y)$ if D_t is Out-of-Distribution (OOD) data, and let us use $\mathbb{P}_{ood}(X, Y)$ to represent the OOD test distribution.

In the classification setting of representation learning, we predict a target $y \in \mathcal{Y}$, where $\mathcal{Y}$ is discrete with K possible categories by using a forecast $h = \sigma(g \circ f)$, which composites a feature extractor $f : \mathcal{X} \to \mathcal{Z}$, where $\mathcal{Z}$ is feature space, a classifier embedding $g : \mathcal{Z} \to \mathbb{R}^K$, and a softmax layer $\sigma : \mathbb{R}^K \to \Delta_y$ which outputs a probability distribution $W(y) : \mathcal{Y} \to [0, 1]$ within the set Δ_y of distributions over $\mathcal{Y}$; the value of probability density function of W is w.

3.2. Method Overview

Toward a reliable and efficient test-time framework, we introduce Density-Softmax. Specifically, to improve uncer-

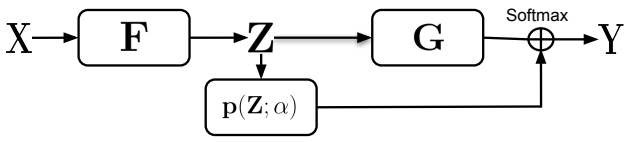

Figure 2. The overall architectures of Density-Softmax, including an encoder f, a classifer g, and a density function $p(Z;\alpha)$. The rectangle boxes represent these functions. The circle with two cross lines represents the softmax layer. The 3 training steps and inference process follow Algorithm 1.

tainty quantification, our idea is based on the solution of the **minimax uncertainty risk** (Meinke & Hein, 2020), i.e.,

$$\inf_{\mathbb{P}(Y|X)\in\mathcal{P}} \left[\sup_{\mathbb{P}^*(Y|X)\in\mathcal{P}^*} S(\mathbb{P}(Y|X), \mathbb{P}^*(Y|X)) \right], \quad (1)$$

where $S(., \mathbb{P}^*(Y|X))$ is strictly proper scoring rules, $\mathbb{P}(Y|X)$ is predictive, and $\mathbb{P}^*(Y|X)$ is the data-generation distribution. When $\mathcal{X}_{ood} = \mathcal{X}/\mathcal{X}_{iid}$, for the Brier Score (Brier, 1950), the solution of the risk was shown by Liu et al. (2020a) as

$$\mathbb{P}(Y|X) = \mathbb{P}(Y|X_{iid})\mathbb{P}^*(X_{iid}) + \mathbb{U}(Y|X_{ood})\mathbb{P}^*(X_{ood}), \quad (2)$$

where X_{iid} is IID, X_{ood} is OOD sample variable, and $\mathbb{U}$ stands for uniform distribution. According to this result, we summarize the overview of Density-Softmax, a solution of the minimax uncertainty risk by Thm. 4.5, in Fig. 2. Under our framework, the predictive distribution is equivalent to

$$\mathbb{P}(Y|X) = \sigma(p(Z;\alpha)\cdot g(Z)), \text{ with } Z = f(X), \quad (3)$$

where $f : \mathcal{X} \to \mathcal{Z}$ is the feature extractor, $g : \mathcal{Z} \to \mathbb{R}^K$ is the last classifier layer, $\sigma : \mathbb{R}^K \to \Delta_y$ is the softmax layer, and $p(Z;\alpha)$ is the density function to measure the distance on feature space $\mathcal{Z}$ with parameter α.

To improve robustness and test-time efficiency, we use the gradient-penalty regularization (Gulrajani et al., 2017) to enforce the feature extractor f to be 1-Lipschitz based on the Rademacher theorem:

Theorem 3.1. *(Federer, 1969) If $f : \mathcal{X} \to \mathcal{Z}$ is a locally Lipschitz continuous function, then f is differentiable almost everywhere. Moreover, if f is Lipschitz continuous, then $L(f) = \sup_{x\in\mathbb{R}^n} ||\nabla_x f(x)||_2$, where $L(f)$ is the Lipschitz constant of f.*

Remark 3.2. The gradient-penalty $(||\nabla_x f(x)||_2 - 1)^2$ enforces $\sup_{x\in\mathbb{R}^n} ||\nabla_x f(x)||_2 = 1$ and Thm. 3.1 suggests $f(x)$ satisfy 1-Lipstchiz constraint by $L(f) = 1$, i.e., $||f(x_1) - f(x_2)||_2 \leq ||x_1 - x_2||_2$ (details are in Apd. B.4). This prevents $f(x)$ from being overly sensitive to the meaningless perturbations of the sample and assures that if the sample is similar, the feature will also be similar. This 1-Lipstchiz $f(x)$ is proved to be robust on the corrupted data by the Local Robustness Certificates property:

Property 3.3. (Tsuzuku et al., 2018) For any 1-Lipschitz $f(x)$, i.e., $L(f) = 1$, the robustness radius ϵ of binary classifier $c = sign \circ f$ at example x verifies $\epsilon \geq ||f(x)||$, where $\epsilon = \min_{\delta\in\mathcal{X}} ||\delta||$ s.t., $c(x+\delta) \neq c(x)$. (This can be generalized to the multi-class case by Béthune et al. (2022)).

3.3. Algorithm

Training. Based on the motivation mentioned above, in the first training step, we optimize the model by using ERM (Vapnik, 1998) and gradient-penalty regularization (Gulrajani et al., 2017) from training data D_s by solving

$$\min_{\theta_{g,f}} \{\mathbb{E}_{(x,y)\sim D_s}[- y \log(\sigma(g(f(x)))) + \lambda(||\nabla_x f(x)||_2 - 1)^2]\}, \quad (4)$$

where $\theta_{g,f}$ is the parameter of encoder f and classifier g, λ is the gradient-penalty coefficient, and $||\nabla_x f(x)||_2$ is the Spectral norm of the Jacobian matrix $\nabla_x f(x)$.

After that, we freeze the parameter θ_f of f to estimate density on the learned representation space $\mathcal{Z}$ by positing a Normalizing-Flows model for $p(Z;\alpha)$ (Papamakarios et al., 2021; Dinh et al., 2017), then fitting MLE to yield α and scale $p(Z;\alpha)$ to a specified range. We use Normalizing-Flows to fit the statistical density model $p(Z;\alpha)$ because it is simple, lightweight, provable, and provides exact log-likelihood (Charpentier et al., 2022). Specifically, we do MLE w.r.t. the logarithm by optimizing

$$\max_{\alpha} \{\mathbb{E}_{(z=f(x))\sim D_s}[\log(p(z;\alpha)) := \log(p(t;\alpha)) + \log\left|\det\left(\frac{\partial t}{\partial z}\right)\right|]\}, \quad (5)$$

where random variable $t = s_\alpha(f(x))$ and s is a bijective differentiable function.

Finally, to enhance generalization after combining with the likelihood value of the density function $p(Z;\alpha)$, we update the weight of classifier g to normalize with the likelihood value by optimizing with the objective function as follows

$$\min_{\theta_g} \left\{\mathbb{E}_{(z=f(x),y)\sim D_s}\left[-y\log\left(\sigma(p(z;\alpha)\cdot g(z))\right)\right]\right\}. \quad (6)$$

Inference. After completing the training process, for a new test sample $x_t \in D_t$ at the test time, we perform prediction by combining the density function on feature space $p(z_t;\alpha)$ and classifier g to predict with only a single forward pass by

Algorithm 1 Density-Softmax: Training and Inference

Training input: Training data D_s, encoder f, density function $p(Z;\alpha)$, classifier g, learning rate η, gradient-penalty coefficient λ.
for $e = 1 \rightarrow$ pre-train epochs **do**
  Sample $(x, y) \in D_B$ with a mini-batch B from D_s
  Update $\theta_{g,f}$ as:

$$\theta_{g,f} - \eta\nabla_{\theta_{g,f}}\mathbb{E}_{(x,y)}[-y\log(\sigma(g(f(x)))) + \lambda(||\nabla_x f(x)||_2 - 1)^2]$$

end for
for $e = 1 \rightarrow$ train-density epochs **do**
  Sample $x \in D_B$ with a mini-batch B from D_s
  Update α as:
  $\alpha - \eta\nabla_\alpha \mathbb{E}_{z=f(x)}\left[-\log(p(t;\alpha)) - \log\left|\det\left(\frac{\partial t}{\partial z}\right)\right|\right]$
end for
Scale: $p(Z;\alpha)$ to $(0, 1]$
for $e = 1 \rightarrow$ re-optimize classifier epochs **do**
  Sample $(x, y) \in D_B$ with a mini-batch B from D_s
  Update θ_g as:
  $\theta_g - \eta\nabla_{\theta_g}\mathbb{E}_{(z=f(x),y)}\left[-y\log(\sigma(p(z;\alpha)\cdot g(z)))\right]$
end for
Inference (test) input: Test sample $x_t \in D_t$
Make a prediction for x_t by following Eq. 7

the following formula

$$p(y = i|x_t) = \frac{\exp(p(z_t;\alpha)\cdot(z_t^\top\theta_{g_i}))}{\sum_{j=1}^{K}\exp(p(z_t;\alpha)\cdot(z_t^\top\theta_{g_j}))}, \forall i \in \mathcal{Y}, \tag{7}$$

where $z_t = f(x_t)$ is the feature of test sample x_t.

Remark 3.4. **(Computational efficiency at test time)** Eq. 7 shows that the complexity of Density-Softmax at test time is similar to Deterministic ERM, i.e., $\mathcal{O}(1)$ by requiring only a single forward pass to produce the softmax probability. Its computation only needs to additionally compute $p(z_t;\alpha)$, therefore, only higher than Deterministic ERM by the additional parameter α and the latency of $p(z_t;\alpha)$. These numbers are often small in practice by the tables in Section 5.

Remark 3.5. **(Disentangling aleatoric and epistemic uncertainty)** Our Eq. 7 returns both aleatoric and epistemic uncertainty. That said, it is still possible to separate these two kinds of uncertainty in our framework. In particular, using the same disentangling technique with DDU (Mukhoti et al., 2023), we can disentangle aleatoric uncertainty by returning the softmax probability without multiplying with the density model in Eq. 7, and epistemic uncertainty by returning the likelihood value of the density model. It is worth noticing that this additional step does not require any retraining step or additional forward passes, hence, does not harm the test-time efficiency.

The pseudo-code for our proposed Density-Softmax framework's training and inference processes is presented in Algorithm 1. Due to the fact that likelihood $p(Z;\alpha) \in (-\infty; +\infty)$, the exponential function in Eq. 7 can return an undefined value if the likelihood $p(Z;\alpha) \rightarrow \infty$. Therefore, we can scale it to the range of $(0, 1]$ to avoid this numerical issue. The detail for controlling the scale of likelihood is provided in Apd B.1.

4. Theoretical Analysis of Uncertainty Estimation

Regarding uncertainty, before presenting the main result, we first recall the definition of distribution calibration (Dawid, 1982) for the forecast:

Definition 4.1. (Song et al., 2019; Kuleshov et al., 2018) A forecast h is said to be **distributional calibrated** if

$$\mathbb{P}(Y = y|h(x) = W) = w(y), \forall y \in \mathcal{Y}, W \in \Delta_y.$$

Intuitively, this means the forecast h is well-calibrated if its outputs truthfully quantify the predictive uncertainty. E.g., if we take all data points x for which the model predicts $[h(x)]_y = 0.3$, we expect 30% of them to indeed take on the label y. To quantify distributional calibrated in Def. 4.1, an approximate estimator of the Calibration Error (Murphy, 1973) in expectation was given by Naeini et al. (2015) and is still the most commonly used measure for a multi-class model. It is referred to as the **Expected Calibration Error (ECE)** of model $h : \mathcal{X} \rightarrow \Delta_y$ is defined as

$$\text{ECE}(h) := \sum_{m=1}^{M}\frac{|B_m|}{N}\left|\text{acc}(B_m) - \text{conf}(B_m)\right|, \tag{8}$$

where B_m is the set of sample indices whose confidence falls into $\left(\frac{m-1}{M}, \frac{m}{M}\right]$ in M bins, N is the number of samples, bin-wise mean accuracy $\text{acc}(B_m) := \frac{1}{|B_m|}\sum_{i\in B_m}\mathbb{I}(\arg\max_{y\in\mathcal{Y}}[h(x_i)]_y = y_i)$, and bin-wise mean confidence $\text{conf}(B_m) := \frac{1}{|B_m|}\sum_{i\in B_m}\max_{y\in\mathcal{Y}}[h(x_i)]_y$.

In addition, let us inherit the definition of Feature Distance Awareness from Liu et al. (2020a):

Definition 4.2. The predictive distribution $\sigma(g(z_t))$ on test feature $z_t = f(x_t)$ is said **feature distance aware** if there exists $u(z_t)$, a summary statistics of $\sigma(g(z_t))$, that quantifies model uncertainty (e.g., entropy, predictive variance, etc.) and reflects the distance between z_t and the training data Z_s w.r.t. $\|\cdot\|_{\mathcal{Z}}$, i.e., $u(z_t) := v(d(z_t, Z_s))$, where v is a monotonic function and $d(z_t, Z_s) := \mathbb{E}\|z_t - Z_s\|_{\mathcal{Z}}$ is the distance between z_t and the training data Z_s.

Then, we recall a Lemma when $p(Z;\alpha)$ is a Normalizing-Flows model (Papamakarios et al., 2021):

Lemma 4.3. *(Charpentier et al., 2022) If $p(Z;\alpha)$ is parametrized with a Gaussian Mixture Models or a radial Normalizing-Flows, then* $\lim_{d(z_t,Z_s)\to\infty} p(z_t;\alpha) \to 0$.

Lemma 4.3 intuitively leads Eq. 7 to reasonable uncertainty estimation for the two limit cases of strong IID and OOD data. In particular, for very unlikely OOD data, i.e., $d(z_t, Z_s) \to \infty$, the prediction will go to uniform. Conversely, for very likely IID data, i.e., $d(z_t, Z_s) \to 0$, the prediction follows the in-domain predictive distribution. Now, we formally show this property below:

Theorem 4.4. *Density-Softmax provides a uniform prediction, i.e., $\sigma(p(z_{ood};\alpha)\cdot g(z_{ood})) = \mathbb{U}$ when $d(z_{ood}, Z_s) \to \infty$ by $p(z_{ood});\alpha) \to 0$, and preserves the in-domain prediction, i.e., $\sigma(p(z_{iid};\alpha)\cdot g(z_{iid})) = \sigma(g(f(x_{iid})))$ when $d(z_{iid}, Z_s) \to 0$ by $p(z_{iid});\alpha) \to 1$. The proof is in Apd. A.1.*

Based on these results, we next show that Density-Softmax is the solution of the minimax uncertainty risk in Eq. (1) and satisfies Def. 4.2 about feature distance awareness:

Theorem 4.5. *Density-Softmax's prediction is the optimal solution of the minimax uncertainty risk, i.e., $\sigma(p(f(X);\alpha)\cdot g(f(X))) = \arg\inf_{\mathbb{P}(Y|X)\in\mathcal{P}} \left[\sup_{\mathbb{P}^*(Y|X)\in\mathcal{P}^*} S(\mathbb{P}(Y|X), \mathbb{P}^*(Y|X))\right]$. The proof is in Apd. A.2.*

Theorem 4.6. *The predictive distribution of Density-Softmax $\sigma(p(z = f(x);\alpha)\cdot(g\circ f(x)))$ is distance aware on the feature space $\mathcal{Z}$ by satisfying the condition in Def. 4.2, i.e., there exists a summary statistic $u(z_t)$ of $\sigma(p(z_t;\alpha)\cdot(g\circ z_t))$ on the new test feature $z_t = f(x_t)$ s.t., $u(z_t) = v(d(z_t, Z_s))$, where v is a monotonic function and $d(z_t, Z_s) = \mathbb{E}\,\|z_t - Z_s\|_{\mathcal{Z}}$ is the distance between z_t and the training features random variable Z_s.*

Proof sketch. Thm. 4.6 is proved by showing (1) $p(z_t = f(x_t);\alpha)$ is monotonically decreasing w.r.t. distance $\mathbb{E}\,\|z_t - Z_s\|_{\mathcal{Z}}$ and (2) $p(z = f(x);\alpha)\cdot g$ is distance aware. Full proof is in Apd. A.3. □

Remark 4.7. Thm. 4.6 shows our Density-Softmax is distance aware on the feature representation $\mathcal{Z}$, i.e., its predictive probability reflects the distance between the test feature and the training set. This is a necessary condition for a DNN to achieve high-quality uncertainty estimation (Liu et al., 2020a). By showing $p(Z;\alpha)$ is monotonically decreasing w.r.t. feature distance, this proves when the likelihood of $p(Z;\alpha)$ is high, our model is certain on IID data, and when the likelihood of $p(Z;\alpha)$ decreases on OOD data, the certainty will decrease correspondingly.

Following these results, we finally present how Density-Softmax can enhance the uncertainty quality of DNN with the standard softmax by reducing its over-confidence in the proposition below:

Proposition 4.8. *If the predictive distribution of the standard softmax $\sigma(g\circ f)$ makes $acc(B_m) \le conf(B_m), \forall B_m, m \in [M]$, where B_m is the set of sample indices whose confidence falls into $\left(\frac{m-1}{M}, \frac{m}{M}\right]$ in M bins, then Density-Softmax $\sigma((p(f;\alpha)\cdot g)\circ f)$ can improve calibrated-uncertainty in terms of ECE in Eq. 8, i.e., $ECE(\sigma((p(f;\alpha)\cdot g)\circ f) \le ECE(\sigma(g\circ f))$. The proof is in Apd. A.4.*

Remark 4.9. The condition $\text{acc}(B_m) \le \text{conf}(B_m), \forall B_m$ is a specific case of the over-confidence for every M bins. And if so, Prop. 4.8 shows Density-Softmax can reduce ECE of the standard softmax, which is also empirically confirmed in Fig. 3 in the next section.

5. Experiments

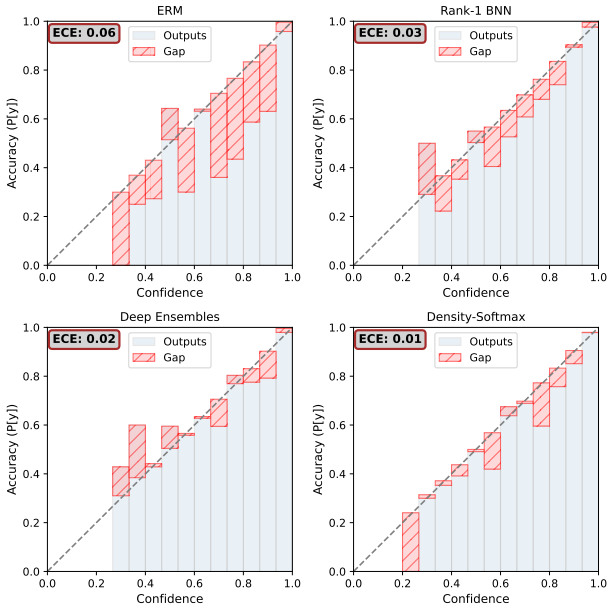

Figure 3. Reliability diagram of Density-Softmax v.s. different approaches, trained on CIFAR-10, test on CIFAR-10.1 (v6). Density-Softmax is better-calibrated than others. Details are in Apd. C.3.3.

We follow experimental settings based on the source code of Nado et al. (2021). Baseline details are in Apd. C.1. Datasets, evaluation metrics, training details, architectures and hyper-parameters, and source code and computing system details are in Apd. C.2. Our source code is available at https://github.com/Angie-Lab-JHU/density_softmax.

Table 2. Results for Wide Resnet-28-10 on CIFAR-10, averaged over 10 seeds: negative log-likelihood (lower is better), accuracy (higher is better), and expected calibration error (lower is better). NLL, Acc, and ECE represent performance on IID test set. cNLL, cAcc, and cECE are NLL, accuracy, and ECE averaged over OOD CIFAR-10-C's corruption types & intensities, oNLL, oAcc, and oECE are for real-world shift CIFAR-10.1. #Params is the number of model parameters, Latency is the milliseconds to inference per sample on RTX A5000, ours is colored by blue (lower are better). Best scores with the significant test are marked in **bold**. Details are in Tab. 8.

Method	NLL(↓)	Acc(↑)	ECE(↓)	cNLL(↓)	cAcc(↑)	cECE(↓)	oNLL(↓)	oAcc(↑)	oECE(↓)	#Params(↓)	Latency(↓)
Deterministic ERM	0.159	96.0	0.023	1.05	76.1	0.153	0.40	89.9	0.064	**36.50M**	**518.12**
Rank-1 BNN	0.128	96.3	**0.008**	0.84	76.7	0.080	0.32	90.4	0.033	36.65M	1,427.67
Heteroscedastic	0.156	96.0	0.023	1.05	76.1	0.154	0.38	90.1	0.056	36.54M	560.43
SNGP	0.134	96.0	0.007	0.74	78.5	0.078	0.43	89.7	0.064	37.50M	916.26
DDU (w/o TS)	0.159	96.0	0.024	1.06	76.0	0.153	0.39	89.8	0.063	37.60M	954.31
NatPN	0.242	92.8	0.041	0.89	73.9	0.121	0.46	86.3	0.049	36.58M	601.35
BatchEnsemble	0.136	96.3	0.018	0.97	77.8	0.124	0.35	90.6	0.048	36.58M	1,498.01
Deep Ensembles	**0.114**	**96.6**	0.010	0.81	77.9	0.087	0.28	**92.2**	0.025	145.99M	1,520.34
Density-Softmax	0.137	96.0	0.010	**0.68**	**79.2**	**0.060**	**0.26**	91.6	**0.016**	36.58M	**520.53**

Table 3. Results for Wide Resnet-28-10 on CIFAR-100: cNLL, cAcc, and cECE are for CIFAR-100-C. AUPR-S and AUPR-C are AUPR for OOD detection on SVHN and CIFAR-10 (higher are better). Details are in Tab. 9.

Method	NLL(↓)	Acc(↑)	ECE(↓)	cNLL(↓)	cAcc(↑)	cECE(↓)	AUPR-S(↑)	AUPR-C(↑)	#Params(↓)	Latency(↓)
Deterministic ERM	0.875	79.8	0.086	2.70	51.4	0.239	0.882	0.745	**36.55M**	**521.15**
Rank-1 BNN	0.692	81.3	**0.018**	2.24	53.8	0.117	0.884	0.797	36.71M	1,448.90
Heteroscedastic	0.833	80.2	0.059	2.40	52.1	0.177	0.881	0.752	37.00M	568.17
SNGP	0.805	80.2	0.020	2.02	54.6	0.092	**0.923**	0.801	37.50M	926.99
DDU (w/o TS)	0.877	79.7	0.086	2.70	51.3	0.240	0.890	0.797	37.60M	959.25
NatPN	1.249	76.9	0.091	2.97	48.0	0.265	0.875	0.768	36.64M	613.44
BatchEnsemble	0.690	81.9	0.027	2.56	53.1	0.149	0.870	0.757	36.63M	1,568.77
Deep Ensembles	**0.666**	**82.7**	0.021	2.27	54.1	0.138	0.888	0.780	146.22M	1,569.23
Density-Softmax	0.780	80.8	0.038	**1.96**	**54.7**	**0.089**	0.910	**0.804**	36.64M	**522.94**

Table 4. Results for Resnet-50 on ImageNet: cNLL, cAcc, and cECE are for ImageNet-C. Details are in Tab. 10.

Method	NLL(↓)	Acc(↑)	ECE(↓)	cNLL(↓)	cAcc(↑)	cECE(↓)	#Params(↓)	Latency(↓)
Deterministic ERM	0.939	76.2	0.032	3.21	40.5	0.103	**25.61M**	**299.81**
Rank-1 BNN	0.886	77.3	0.017	2.95	42.9	0.054	26.35M	690.14
Heteroscedastic	0.898	77.5	0.033	3.20	42.4	0.111	58.39M	337.50
SNGP	0.931	76.1	**0.013**	3.03	41.1	0.045	26.60M	606.11
MIMO	0.887	77.5	0.037	3.03	43.3	0.106	27.67M	367.17
BatchEnsemble	0.922	76.8	0.037	3.09	41.9	0.089	25.82M	696.81
Deep Ensembles	**0.857**	**77.9**	0.017	2.82	**44.9**	0.047	102.44M	701.34
Density-Softmax	0.885	77.5	0.019	**2.81**	44.6	**0.042**	25.88M	**299.90**

5.1. Robustness Performance

Density-Softmax achieves competitive robust generalization with SOTA. Tab. 2, 3, and 4 show benchmark results across shifted datasets. We observe Density-Softmax achieve a competitive result with the State-of-the-art (SOTA) in NLL and accuracy under distribution shifts. Specifically, our method has the lowest NLL and highest accuracy with $0.68, 79.2\%$, $1.96, 54.7\%$, and $2.81, 44.6\%$ respectively in the corrupted OOD datasets CIFAR-10-C, CIFAR-100-C, and ImageNet-C. Regarding the real-world shift CIFAR-10.1, it also achieves the lowest NLL with 0.26, and 91.6% in accuracy, higher than other methods and only lower than Deep Ensembles by 0.6%. Although there is a trade-off between IID and OOD performance by the Lipschitz constraint in Apd. B.3, it is also worth noticing that with an appropriate λ, our method can still preserve a high accuracy in IID at the same time and outperforms many baselines. E.g., it achieves 77.5% in ImageNet, higher than Deterministc ERM, Rank-1 BNN, SNGP, BatchEnsemble, etc. More details about benchmark comparison are in Apd. C.3.2.

5.2. Uncertainty Estimation Performance

Density-Softmax achieves competitive uncertainty performances with SOTA. From the tables, we also observe our model has a competitive uncertainty quality and even sometimes outperforms the SOTA like Rank-1 BNN, SNGP, and Deep Ensembles, especially under OOD settings. E.g., it achieves the lowest cECE with 0.060 in CIFAR-10-C, 0.089 in CIFAR-100-C, and 0.042 in ImageNet-C. Similarly, it has the best AUPR-C with 0.804 in CIFAR-10 and 0.016 oECE in CIFAR-10.1.

To take a closer look at the calibration, we visualize reliability diagrams based on the ECE in Fig. 3. We observe that Density-Softmax is better calibrated than other methods

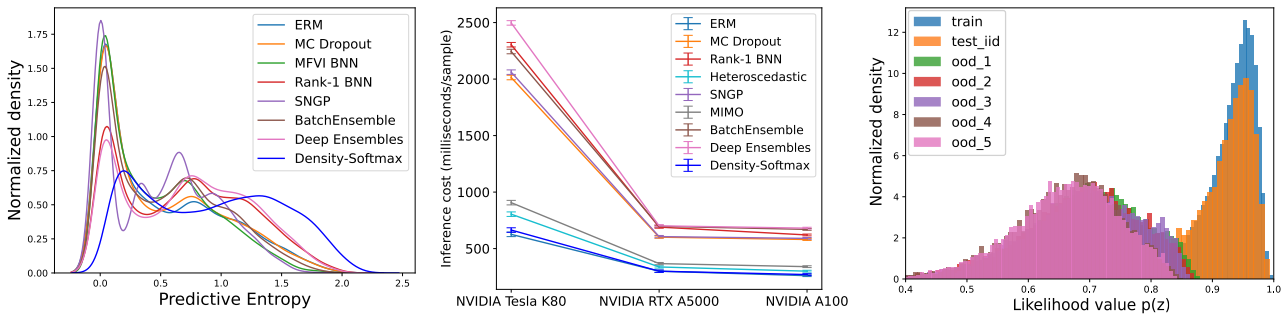

(a) (b) (c)

Figure 4. (a) PDF plot of predictive entropy $\mathrm{H}(p(y|x))$ for the semantic shift. Density-Softmax provides the highest entropy with high density for OOD; (b) Inference cost comparison at test time on ImageNet. Our model consistently outperforms SOTA across modern GPU architectures; (c) Histogram of $p(z;\alpha)$'s likelihood. Blue represents on CIFAR-10 train, Orange is IID test, Green, Red, Purple, Brown, Pink are OOD from 1-5 shift levels on CIFAR-10-C. It produces high values on IID and lower values on OOD w.r.t. intensity levels.

in the real-world shifted OOD test set. E.g., compared to Deterministic ERM, our model is less over-confident, confirming Prop. 4.8. Meanwhile, compared to Rank-1 BNN and Deep Ensembles, it is less under-confidence. Calibration details with reliability diagrams in both IID and OOD are in Apd. C.3.3.

Density-Softmax achieves distance awareness. From Fig. 1, we observe that our model achieves distance awareness by having uniform class probability and high uncertainty value on OOD data on the two moons dataset, confirming Thm. 4.6. Meanwhile, Deterministic ERM, MC Dropout, Rank-1 BNN, and Ensembles can not provide distance awareness as they provide no informative variance for OOD data. Similar observations are in Apd. C.3.1 with different uncertainty metrics and datasets.

Density-Softmax produces high entropy on OOD and low entropy on IID data under semantic shift. Fig. 4 (a) compares the density of predictive entropy between different methods trained on CIFAR-10 and tested on CIFAR-100. Because this is the semantic shift (Tran et al., 2022), we would expect the model to provide a high entropy value. Indeed, we observe that Density-Softmax achieves the highest entropy with a high-density value. In Fig. 17 in Apd. C.3.4, we also observe that our model preserves low entropy with high-density value on IID data, confirming the hypothesis that our framework can enhance uncertainty quantification. More details about the histograms are in Apd. C.3.4.

Density-Softmax outperforms SOTA in inference speed. Our method only requires one forward pass to make a prediction, so it outperforms other SOTA in terms of inference speed. For every dataset with different backbones, we observe that Density-Softmax achieves almost the same latency with Deterministic ERM. In particular, it takes less than 525 and 300 ms/sample in Wide Resnet-28-10 and Resnet-50 for an inference on RTX A5000. To make a further comparison on test-time latency, we compare the running time on 3 modern GPU architectures in Fig. 4 (b). We observe that our model consistency outperforms SOTA, especially for lower computational hardware like NVIDIA Tesla K80.

Having a similar latency, the tables show our model is also more reliable than Deterministic ERM by always achieving a lower NLL, ECE, and higher accuracy. Therefore, these results suggest that Density-Softmax could be a potential deterministic approach for uncertainty and robustness in real-time applications.

Density-Softmax outperforms SOTA in storage requirements. From the tables, the parameters and latency of $p(Z;\alpha)$ can be measured by the minus of ours to Deterministic ERM by Re. 3.4. We observe that Density-Softmax is very lightweight with less than 36.65M parameters in Wide Resnet-28-10 and 25.88M in Resnet-50. These numbers are lower than other SOTA baselines, e.g., Rank-1 BNN, Heteroscedastic, SNGP, MIMO, and Deep Ensembles with Resnet-50 on ImagetNet.

In summary, combined with the latency performance, Density-Softmax outperforms other SOTA approaches in computational efficiency at the test time. In particular, our model is less than Deep Ensembles by 4 times in the number of parameters. Regarding the latency, Density-Softmax is also much faster than other SOTA baselines across different hardware architectures.

5.3. Ablation study: Analysis of Density Softmax's components

How does Density Softmax work? Our framework is a combination of 2 main components: (1) the Lipschitz-constrained f and (2) the density function $p(Z;\alpha)$. To test their importance, we compare architectures with and without each component in our model. From Fig. 5, we observe

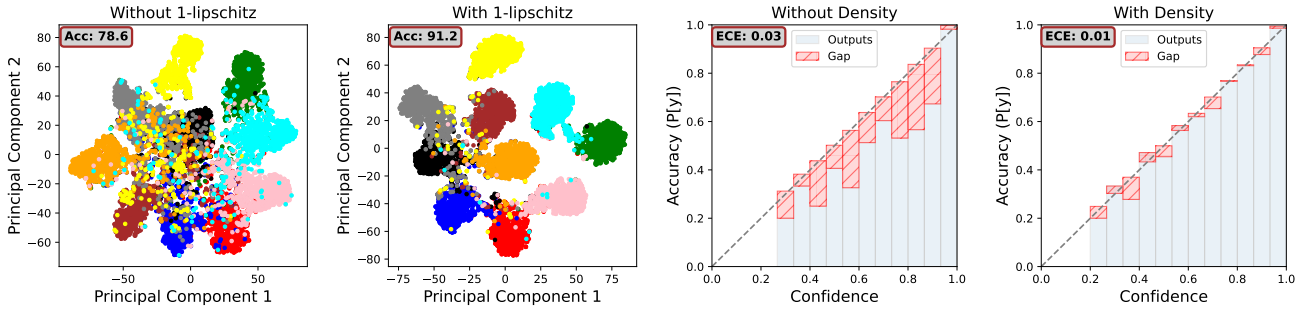

(a) (b) (c) (d)

Figure 5. Feature visualizations comparison between models with & without 1-Lipschitz constraint on CIFAR-10-C (a & b), reliability diagrams between models with & without the density-function on CIFAR-10 (c & d).

that without the 1-Lipschitz regularization, the model has a worse feature representation than (1), e.g., leading to a drop in the accuracy from 91.2% to 78.6% on the CIFAR-10-C with defocus_blur_5. Similarly, without $p(Z;\alpha)$, the model has a worse uncertainty quality than (2), e.g., causing an increase in the ECE from 0.01 to 0.03 on CIFAR-10. These results prove that the Lipschitz-constrained f helps our model improve robustness, while the density function $p(Z;\alpha)$ enhances the uncertainty quantification. Last but not least, we discover that Lipschitz-constrained f not only improves the robustness but also the uncertainty quality by observing a worse ECE performance without the Lipschitz constraint, i.e., $\lambda = 0$ in Tab. 5.

Our density model can capture distributional shifts. Density-Softmax estimates the density on the low-dimensional feature space $\mathcal{Z}$, which is fixed after the first step of Algorithm 1. This feature structure is low-dimensional, task-specific, and encodes meaningful semantic features (Manh Bui & Liu, 2024; Charpentier et al., 2022). Therefore, this feature space $\mathcal{Z}$ is much simpler to estimate when compared to the complex image pixels space $\mathcal{X}$. We visualize the likelihood histogram of our Normalizing-Flows density function across training, IID testing, and OOD sets in Fig. 4 (c). We observe that our density function provides a high likelihood for IID while low values for OOD test set. Importantly, when the shift intensity increases, the likelihood also decreases, showing that our model can reduce certainty correspondingly.

6. Conclusion and Discussion

Despite showing success in reliable DNN, sampling-based methods like Deep Ensembles and BNN suffer from huge computational burdens at test-time. To tackle this challenge, we introduce Density-Softmax, a sampling-free approach to improve uncertainty and robustness via a combination of a feature density function from the Lipschitz-constrained feature extractor with the softmax layer. We complement this algorithm with a theoretical analysis establishing guarantees on the 1-Lipschitz constraint, solution of the minimax uncertainty risk, distance awareness on feature space, and reducing over-confidence of the standard softmax. Empirically, we find our proposed framework achieves competitive results with SOTA methods in uncertainty and robustness while outperforming them significantly in terms of memory and inference cost at test-time. We hope that our work will be an option for developers to try in real-world applications and inspire researchers to further progress in the area of improving the DNN model efficiency and reliability.

Density model performance in practice. The uncertainty quality of our method depends on the density function. Our results show if the likelihood on test OOD feature is lower than IID set, then Density-Softmax can reduce the over-confidence of the standard softmax. Yet, it can be a risk that our model might not fully capture the real-world complexity by estimating density model is not always trivial in practice (Nalisnick et al., 2019; Charpentier et al., 2022).

Training cost. Despite showing success in test-time efficiency, we also ask users to be cautious about the longer training time of our Density-Softmax than Deterministic ERM in practice (details are in Apd. B.3).

Remediation. Given the aforementioned limitations, we encourage people who extend our work to: (1) proactively confront the model design and parameters to desired behaviors in real-world use cases; (2) be aware of the training challenge and prepare enough time and resources (e.g., setting enough GPU servers, training on GPU cloud services, etc.) to pre-train our framework in practice.

Future work. Future work includes providing uncertainty estimates for pre-trained large models (details are in Apd. B.4), developing new techniques to avoid computing the Jacobian matrix at training time, improving estimation techniques to enhance the quality of the density function, and continuing to reduce the number of parameters to deploy this framework in real-world systems.

Impact Statement

Uncertainty & robustness are critical problems in trustworthy AI. There has been growing interest in using sampling-based methods to ensure DNN are robust and reliable. Challenges often arise when deploying such models in real-world applications. In this regard, Density-Softmax significantly improves test-time efficiency while preserving reliability. This could be particularly beneficial in high-stake applications (e.g., healthcare, finance, policy decision-making, etc.), where the trained model needs to be deployed and inference on low-resource hardware or real-time response software.

Acknowledgments

This work is partially supported by the JHU-Amazon AI2AI faculty award, the Discovery Award of the Johns Hopkins University, and a seed grant from JHU Institute of Assured Autonomy.

References

Béthune, L., Boissin, T., Serrurier, M., Mamalet, F., Friedrich, C., and Gonzalez Sanz, A. Pay attention to your loss : understanding misconceptions about lipschitz neural networks. In *Advances in Neural Information Processing Systems*, 2022.

Blundell, C., Cornebise, J., Kavukcuoglu, K., and Wierstra, D. Weight uncertainty in neural networks. In *Proceedings of the 32nd International Conference on Machine Learning*, 2015.

Brier, G. W. Verification of Forecasts Expressed in Terms of Probability. *Monthly Weather Review*, 1950.

Bröcker, J. Reliability, sufficiency, and the decomposition of proper scores. *Quarterly Journal of the Royal Meteorological Society*, 2009.

Bui, H. M. and Maifeld-Carucci, I. Benchmark for uncertainty & robustness in self-supervised learning, 2022.

Bui, M.-H., Tran, T., Tran, A., and Phung, D. Exploiting domain-specific features to enhance domain generalization. In *Advances in Neural Information Processing Systems*, 2021.

Carratino, L., Cissé, M., Jenatton, R., and Vert, J.-P. On mixup regularization. *J. Mach. Learn. Res.*, 2022.

Charpentier, B., Zügner, D., and Günnemann, S. Posterior network: Uncertainty estimation without ood samples via density-based pseudo-counts. In *Advances in Neural Information Processing Systems*, 2020.

Charpentier, B., Borchert, O., Zügner, D., Geisler, S., and Günnemann, S. Natural posterior network: Deep bayesian predictive uncertainty for exponential family distributions. In *International Conference on Learning Representations*, 2022.

Chen, Y., Yuan, L., Cui, G., Liu, Z., and Ji, H. A close look into the calibration of pre-trained language models, 2022.

Collier, M., Mustafa, B., Kokiopoulou, E., Jenatton, R., and Berent, J. Correlated input-dependent label noise in large-scale image classification. In *Proceedings of the IEEE/CVF Conference on Computer Vision and Pattern Recognition (CVPR)*, 2021.

Dawid, A. P. The well-calibrated bayesian. *Journal of the American Statistical Association*, 1982.

Dinh, L., Sohl-Dickstein, J., and Bengio, S. Density estimation using real NVP. In *International Conference on Learning Representations*, 2017.

Dosovitskiy, A., Beyer, L., Kolesnikov, A., Weissenborn, D., Zhai, X., Unterthiner, T., Dehghani, M., Minderer, M., Heigold, G., Gelly, S., Uszkoreit, J., and Houlsby, N. An image is worth 16x16 words: Transformers for image recognition at scale. In *International Conference on Learning Representations*, 2021.

Dusenberry, M., Jerfel, G., Wen, Y., Ma, Y., Snoek, J., Heller, K., Lakshminarayanan, B., and Tran, D. Efficient and scalable Bayesian neural nets with rank-1 factors. In *Proceedings of the 37th International Conference on Machine Learning*, 2020.

Federer, H. *Geometric measure theory*. Classics in Mathematics. Springer-Verlag Berlin Heidelberg, 1969.

Gal, Y. and Ghahramani, Z. A theoretically grounded application of dropout in recurrent neural networks. In *Advances in Neural Information Processing Systems*, 2016a.

Gal, Y. and Ghahramani, Z. Dropout as a bayesian approximation: Representing model uncertainty in deep learning. In *Proceedings of The 33rd International Conference on Machine Learning*, 2016b.

Gal, Y., Hron, J., and Kendall, A. Concrete dropout. In *Advances in Neural Information Processing Systems*, 2017.

Gardner, J., Pleiss, G., Weinberger, K. Q., Bindel, D., and Wilson, A. G. Gpytorch: Blackbox matrix-matrix gaussian process inference with gpu acceleration. In *Advances in Neural Information Processing Systems*, 2018.

Gneiting, T. and Raftery, A. E. Strictly proper scoring rules, prediction, and estimation. *Journal of the American Statistical Association*, 2007.

Goodfellow, I. J., Bengio, Y., and Courville, A. *Deep Learning*. MIT Press, Cambridge, MA, USA, 2016.

Gouk, H., Frank, E., Pfahringer, B., and Cree, M. J. Regularisation of neural networks by enforcing lipschitz continuity. *Mach. Learn.*, 2021.

Grünwald, P. D. and Dawid, A. P. Game theory, maximum entropy, minimum discrepancy and robust Bayesian decision theory. *The Annals of Statistics*, 2004.

Gulrajani, I., Ahmed, F., Arjovsky, M., Dumoulin, V., and Courville, A. C. Improved training of wasserstein gans. In *Advances in Neural Information Processing Systems*, 2017.

Guo, C., Pleiss, G., Sun, Y., and Weinberger, K. Q. On calibration of modern neural networks. In *Proceedings of the 34th International Conference on Machine Learning*, 2017.

Havasi, M., Jenatton, R., Fort, S., Liu, J. Z., Snoek, J., Lakshminarayanan, B., Dai, A. M., and Tran, D. Training independent subnetworks for robust prediction. In *International Conference on Learning Representations*, 2021.

He, K., Zhang, X., Ren, S., and Sun, J. Deep residual learning for image recognition. In *2016 IEEE Conference on Computer Vision and Pattern Recognition (CVPR)*, 2016.

Hendrycks, D. and Dietterich, T. Benchmarking neural network robustness to common corruptions and perturbations. In *International Conference on Learning Representations*, 2019.

Hendrycks*, D., Mu*, N., Cubuk, E. D., Zoph, B., Gilmer, J., and Lakshminarayanan, B. Augmix: A simple method to improve robustness and uncertainty under data shift. In *International Conference on Learning Representations*, 2020.

Hinton, G., Vinyals, O., and Dean, J. Distilling the knowledge in a neural network. In *NIPS Deep Learning and Representation Learning Workshop*, 2015.

Karandikar, A., Cain, N., Tran, D., Lakshminarayanan, B., Shlens, J., Mozer, M. C., and Roelofs, B. Soft calibration objectives for neural networks. In *Advances in Neural Information Processing Systems*, 2021.

Kingma, D. P. and Ba, J. Adam: A method for stochastic optimization. In *3rd International Conference on Learning Representations, ICLR 2015, San Diego, CA, USA, May 7-9, 2015, Conference Track Proceedings*, 2015.

Kopetzki, A.-K., Charpentier, B., Zügner, D., Giri, S., and Günnemann, S. Evaluating robustness of predictive uncertainty estimation: Are dirichlet-based models reliable ? In *International Conference on Machine Learning*, 2021.

Kotelevskii, N., Artemenkov, A., Fedyanin, K., Noskov, F., Fishkov, A., Shelmanov, A., Vazhentsev, A., Petiushko, A., and Panov, M. Nonparametric uncertainty quantification for single deterministic neural network. In *Advances in Neural Information Processing Systems*, 2022.

Kristiadi, A., Hein, M., and Hennig, P. Being bayesian, even just a bit, fixes overconfidence in ReLU networks. In *Proceedings of the 37th International Conference on Machine Learning*, 2020.

Kuleshov, V. and Deshpande, S. Calibrated and sharp uncertainties in deep learning via density estimation. In *Proceedings of the 39th International Conference on Machine Learning*, 2022.

Kuleshov, V., Fenner, N., and Ermon, S. Accurate uncertainties for deep learning using calibrated regression. In *Proceedings of the 35th International Conference on Machine Learning*, 2018.

Lakshminarayanan, B., Pritzel, A., and Blundell, C. Simple and scalable predictive uncertainty estimation using deep ensembles. In *Advances in Neural Information Processing Systems*, 2017.

Lee, J., Sohl-dickstein, J., Pennington, J., Novak, R., Schoenholz, S., and Bahri, Y. Deep neural networks as gaussian processes. In *International Conference on Learning Representations*, 2018a.

Lee, K., Lee, K., Lee, H., and Shin, J. A simple unified framework for detecting out-of-distribution samples and adversarial attacks. In *Advances in Neural Information Processing Systems*, 2018b.

Li, Q., Haque, S., Anil, C., Lucas, J., Grosse, R. B., and Jacobsen, J.-H. Preventing gradient attenuation in lipschitz constrained convolutional networks. In *Advances in Neural Information Processing Systems*, 2019.

Liu, J., Lin, Z., Padhy, S., Tran, D., Bedrax Weiss, T., and Lakshminarayanan, B. Simple and principled uncertainty estimation with deterministic deep learning via distance awareness. In *Advances in Neural Information Processing Systems*, 2020a.

Liu, W., Wang, X., Owens, J., and Li, Y. Energy-based out-of-distribution detection. In *Advances in Neural Information Processing Systems*, 2020b.

Maddox, W. J., Izmailov, P., Garipov, T., Vetrov, D. P., and Wilson, A. G. A simple baseline for bayesian uncertainty in deep learning. In *Advances in Neural Information Processing Systems*, 2019.

Malinin, A. and Gales, M. Predictive uncertainty estimation via prior networks. In *Advances in Neural Information Processing Systems*, 2018.

Malinin, A. and Gales, M. Reverse kl-divergence training of prior networks: Improved uncertainty and adversarial robustness. In *Advances in Neural Information Processing Systems*, 2019.

Malinin, A., Mlodozeniec, B., and Gales, M. Ensemble distribution distillation. In *International Conference on Learning Representations*, 2020.

Manh Bui, H. and Liu, A. Density-regression: Efficient and distance-aware deep regressor for uncertainty estimation under distribution shifts. In *Proceedings of The 27th International Conference on Artificial Intelligence and Statistics*, 2024.

Meinke, A. and Hein, M. Towards neural networks that provably know when they don't know. In *International Conference on Learning Representations*, 2020.

Minderer, M., Djolonga, J., Romijnders, R., Hubis, F., Zhai, X., Houlsby, N., Tran, D., and Lucic, M. Revisiting the calibration of modern neural networks. In *Advances in Neural Information Processing Systems*, 2021.

Miyato, T., Kataoka, T., Koyama, M., and Yoshida, Y. Spectral normalization for generative adversarial networks. In *International Conference on Learning Representations*, 2018.

Mukhoti, J., Kirsch, A., van Amersfoort, J., Torr, P. H., and Gal, Y. Deep deterministic uncertainty: A new simple baseline. In *Proceedings of the IEEE/CVF Conference on Computer Vision and Pattern Recognition*, 2023.

Murphy, A. H. A new vector partition of the probability score. *Journal of Applied Meteorology*, 1973.

Nado, Z., Band, N., Collier, M., Djolonga, J., Dusenberry, M., Farquhar, S., Filos, A., Havasi, M., Jenatton, R., Jerfel, G., Liu, J., Mariet, Z., Nixon, J., Padhy, S., Ren, J., Rudner, T., Wen, Y., Wenzel, F., Murphy, K., Sculley, D., Lakshminarayanan, B., Snoek, J., Gal, Y., and Tran, D. Uncertainty Baselines: Benchmarks for uncertainty & robustness in deep learning. *arXiv preprint arXiv:2106.04015*, 2021.

Naeini, M. P., Cooper, G. F., and Hauskrecht, M. Obtaining well calibrated probabilities using bayesian binning. In *Proceedings of the Twenty-Ninth AAAI Conference on Artificial Intelligence*, 2015.

Nalisnick, E., Matsukawa, A., Teh, Y. W., Gorur, D., and Lakshminarayanan, B. Do deep generative models know what they don't know? In *International Conference on Learning Representations*, 2019.

Netzer, Y., Wang, T., Coates, A., Bissacco, A., Wu, B., and Ng, A. Y. Reading digits in natural images with unsupervised feature learning. In *NIPS Workshop on Deep Learning and Unsupervised Feature Learning 2011*, 2011.

Ovadia, Y., Fertig, E., Ren, J., Nado, Z., Sculley, D., Nowozin, S., Dillon, J., Lakshminarayanan, B., and Snoek, J. Can you trust your model's uncertainty? evaluating predictive uncertainty under dataset shift. In *Advances in Neural Information Processing Systems*, 2019.

Papamakarios, G., Nalisnick, E., Rezende, D. J., Mohamed, S., and Lakshminarayanan, B. Normalizing flows for probabilistic modeling and inference. *Journal of Machine Learning Research*, 2021.

Parry, M., Dawid, A. P., and Lauritzen, S. Proper local scoring rules. *The Annals of Statistics*, 2012.

Recht, B., Roelofs, R., Schmidt, L., and Shankar, V. Do cifar-10 classifiers generalize to cifar-10?, 2018.

Riquelme, C., Tucker, G., and Snoek, J. Deep bayesian bandits showdown: An empirical comparison of bayesian deep networks for thompson sampling. In *International Conference on Learning Representations*, 2018.

Searcód, M. O. *Metric Spaces*. Springer London, London, 2007 edition edition, August 2006. ISBN 978-1-84628-369-7.

Sensoy, M., Kaplan, L., and Kandemir, M. Evidential deep learning to quantify classification uncertainty. In *Advances in Neural Information Processing Systems*, 2018.

Snoek, J., Rippel, O., Swersky, K., Kiros, R., Satish, N., Sundaram, N., Patwary, M., Prabhat, M., and Adams, R. Scalable bayesian optimization using deep neural networks. In *Proceedings of the 32nd International Conference on Machine Learning*, 2015.

Song, H., Diethe, T., Kull, M., and Flach, P. Distribution calibration for regression. In *Proceedings of the 36th International Conference on Machine Learning*, 2019.

Sun, Y., Ming, Y., Zhu, X., and Li, Y. Out-of-distribution detection with deep nearest neighbors. In *Proceedings of the 39th International Conference on Machine Learning*, 2022.

Tagasovska, N. and Lopez-Paz, D. Single-model uncertainties for deep learning. In *Advances in Neural Information Processing Systems*, 2019.

Tran, D., Liu, J., Dusenberry, M. W., Phan, D., Collier, M., Ren, J., Han, K., Wang, Z., Mariet, Z., Hu, H., Band, N., Rudner, T. G. J., Singhal, K., Nado, Z., van Amersfoort, J., Kirsch, A., Jenatton, R., Thain, N., Yuan, H., Buchanan, K., Murphy, K., Sculley, D., Gal, Y., Ghahramani, Z., Snoek, J., and Lakshminarayanan, B. Plex: Towards reliability using pretrained large model extensions, 2022.

Tsuzuku, Y., Sato, I., and Sugiyama, M. Lipschitz-margin training: Scalable certification of perturbation invariance for deep neural networks. In *Advances in Neural Information Processing Systems*, 2018.

Vadera, M., Jalaian, B., and Marlin, B. Generalized bayesian posterior expectation distillation for deep neural networks. In *Proceedings of the 36th Conference on Uncertainty in Artificial Intelligence (UAI)*, 2020.

Van Amersfoort, J., Smith, L., Teh, Y. W., and Gal, Y. Uncertainty estimation using a single deep deterministic neural network. In *Proceedings of the 37th International Conference on Machine Learning*, 2020.

van Amersfoort, J., Smith, L., Jesson, A., Key, O., and Gal, Y. On feature collapse and deep kernel learning for single forward pass uncertainty, 2022.

Vapnik, V. N. *Statistical Learning Theory*. Wiley-Interscience, 1998.

Virmaux, A. and Scaman, K. Lipschitz regularity of deep neural networks: analysis and efficient estimation. In *Advances in Neural Information Processing Systems*, 2018.

Wang, H., Li, Z., Feng, L., and Zhang, W. Vim: Out-of-distribution with virtual-logit matching. In *Proceedings of the IEEE/CVF Conference on Computer Vision and Pattern Recognition (CVPR)*, 2022.

Wei, H., Xie, R., Cheng, H., Feng, L., An, B., and Li, Y. Mitigating neural network overconfidence with logit normalization. In *International Conference on Machine Learning (ICML)*, 2022.

Wen, Y., Vicol, P., Ba, J., Tran, D., and Grosse, R. Flipout: Efficient pseudo-independent weight perturbations on mini-batches. In *International Conference on Learning Representations*, 2018.

Wen, Y., Tran, D., and Ba, J. Batchensemble: an alternative approach to efficient ensemble and lifelong learning. In *International Conference on Learning Representations*, 2020.

Zagoruyko, S. and Komodakis, N. Wide residual networks. In *Proceedings of the British Machine Vision Conference (BMVC)*, 2016.

Zhang, H., Cisse, M., Dauphin, Y. N., and Lopez-Paz, D. mixup: Beyond empirical risk minimization. In *International Conference on Learning Representations*, 2018.

Acronyms

AUPR Area Under the Precision-Recall.

AUROC Area Under the Receiver Operating Characteristic.

BNN Bayesian Neural Network.

DDU Deep Deterministic Uncertainty.

DNN Deep Neural Network.

DUE Deterministic Uncertainty Estimation.

DUQ Deterministic Uncertainty Quantification.

ECE Expected Calibration Error.

ERM Empirical Risk Minimization.

IID Independent-identically-distributed.

MC Monte-Carlo.

MFVI Mean-Field Variational Inference.

MIMO Multi-input Multi-output.

MLE Maximum Likelihood Estimation.

NatPN Natural Posterior Network.

NLL Negative log-likelihood.

OOD Out-of-Distribution.

SNGP Spectral-normalized Neural Gaussian Process.

SOTA State-of-the-art.

Density-Softmax: Efficient Test-time Model for Uncertainty Estimation and Robustness under Distribution Shifts (Supplementary Material)

Reproducibility. Our code inherits from the uncertainty-baselines codebase, so our reported results could be referred from this page. In Apd. C, we provide detailed information about our experiments, including baseline in Apd. C.1, implementation in Apd. C.2, and additional results in Apd. C.3. The additional results in Apd. C.3 contain results for the toy dataset in Apd. C.3.1, results for the benchmark dataset in Apd. C.3.2, uncertainty details about calibration in Apd. C.3.3, and about predictive entropy in Apd. C.3.4. In Apd. B, we make further discussions about our method, including density estimation and likelihood value implementation in Apd. B.1, distance preserving and 1-Lipschitz constraint in Apd. B.2, additional ablation study about the gradient-penalty and training cost in Apd. B.3, and additional discussion about our method in Apdx. B.4. Finally, in Apd. A, we provide the proofs for all the results in the main paper, including proof of Thm. 4.4 in Apd. A.1, proof of Thm. 4.5 in Apd. A.2, proof of Thm. 4.6 in Apd. A.3, and proof of Prop. 4.8 in Apd. A.4.

A. Proofs

In this appendix, we provide proof of the theoretical results from the main paper.

A.1. Proof of Theorem 4.4

The proof contains two parts. The first part shows Density-Softmax provides a uniform prediction when $d(z_{ood}, Z_s) \to \infty$. The second part shows Density-Softmax preserves the in-domain prediction when $d(z_{iid}, Z_s) \to 0$.

Part (1). Density-Softmax provides a uniform prediction when $d(z_{ood}, Z_s) \to \infty$:

Proof. Consider the non-uniform in predictive distribution $\sigma(g(f(x_{ood}))) \neq \mathbb{U}$, we have

$$p(y = i|x_{ood}) = \frac{\exp(z_{ood}^\top \theta_{g_i})}{\sum_{j=1}^K \exp(z_{ood}^\top \theta_{g_j})} \neq \frac{1}{K}, \forall i \in \mathcal{Y}, \tag{9}$$

where $z_{ood} = f(x_{ood})$ is the latent presentation for test sample x_{ood}, K is the total of the number of categorical in the discrete label space $\mathcal{Y}$.

Let us rewrite the Density-Softmax predictive distribution $\sigma(p(z_{ood}; \alpha) \cdot g(z_{ood}))$ by

$$p(y = i|x_{ood}) = \frac{\exp(p(z_{ood}; \alpha) \cdot (z_{ood}^\top \theta_{g_i})}{\sum_{j=1}^K \exp(p(z_{ood}; \alpha) \cdot (z_{ood}^\top \theta_{g_j}))}, \forall i \in \mathcal{Y}. \tag{10}$$

Using Lemma 4.3, we have $\lim_{d(z_t, Z_s) \to \infty} p(z_t; \alpha) \to 0$, i.e., if $d(z_{ood}, Z_s) \to \infty$ then $p(z_{ood}; \alpha) \to 0$. Therefore, we obtain

$$\lim_{p(z_{ood}; \alpha) \to 0} \exp(p(z_{ood}; \alpha) \cdot (z_{ood}^\top \theta_{g_i})) = e^0 = 1, \forall i \in \mathcal{Y}. \tag{11}$$

Since $\exp(p(z_{ood}; \alpha) \cdot (z_{ood}^\top \theta_{g_j})) = 1, \forall j \in \mathcal{Y}$ when $p(z_{ood}; \alpha) \to 0$, then

$$p(y = i|x_{ood}) = \frac{\exp(p(z_{ood}; \alpha) \cdot (z_{ood}^\top \theta_{g_i}))}{\sum_{j=1}^K \exp(p(z_{ood}; \alpha) \cdot (z_{ood}^\top \theta_{g_j}))} = \frac{1}{\sum_{i=1}^K 1} = \frac{1}{K}, \forall i \in \mathcal{Y}. \tag{12}$$

As a consequence, when $d(z_{ood}, Z_s) \to \infty$, we obtain the conclusion: $\sigma(p(z_{ood}; \alpha) \cdot g(z_{ood})) = \mathbb{U}$, where $\mathbb{U}$ stands for uniform distribution of Theorem 4.4.

Part (2). Density-Softmax preserves the in-domain prediction when $d(z_{iid}, Z_s) \to 0$:

Consider Density-Softmax predictive distribution $\sigma(p(z_{iid};\alpha)\cdot g(z_{iid}))$, we have

$$p(y=i|x_{iid}) = \frac{\exp(p(z_{iid};\alpha)\cdot(z_{iid}^\top\theta_{g_i}))}{\sum_{j=1}^K \exp(p(z_{iid};\alpha)\cdot(z_{iid}^\top\theta_{g_j}))}, \forall i \in \mathcal{Y}. \tag{13}$$

Due to the likelihood value of $p(Z;\alpha)$ is scale in the range of $(0,1]$, we have $\lim_{d(z_t,Z_s)\to 0} p(z_t;\alpha) \to 1$, i.e., if $d(z_{iid}, Z_s) \to 0$ then $p(z_{iid};\alpha) \to 1$. Therefore, we obtain

$$\lim_{p(z_{iid};\alpha)\to 1} \exp(p(z_{iid};\alpha)\cdot(z_{iid}^\top\theta_{g_i})) = \exp(z_{iid}^\top\theta_{g_i}), \forall i \in \mathcal{Y}. \tag{14}$$

Since $\exp(p(z_{iid};\alpha)\cdot(z_{iid}^\top\theta_{g_i})) = \exp(z_{iid}^\top\theta_{g_i}), \forall i \in \mathcal{Y}$ when $p(z_{iid};\alpha)\to 1$, then

$$p(y=i|x_{iid}) = \frac{\exp(p(z_{iid};\alpha)\cdot(z_{iid}^\top\theta_{g_i}))}{\sum_{j=1}^K \exp(p(z_{iid};\alpha)\cdot(z_{iid}^\top\theta_{g_j}))} = \frac{\exp(z_{iid}^\top\theta_{g_i})}{\sum_{j=1}^K \exp(z_{iid}^\top\theta_{g_j})}, \forall i \in \mathcal{Y}. \tag{15}$$

As a consequence, when $d(z_{iid}, Z_s) \to 0$, we obtain the conclusion: $\sigma(p(z_{iid};\alpha)\cdot g(z_{iid})) = \sigma(g(f(x_{iid})))$ of Theorem 4.4. □

A.2. Proof of Theorem 4.5

Proof. This proof is based on the following provable Lemma of Liu et al. (2020a):

Lemma A.1. *(Liu et al., 2020a; Grünwald & Dawid, 2004)* ***(The uniform distribution $\mathbb{U}$ is the optimal for minimax Bregman score in $x \notin \mathcal{X}_{iid}$).*** *Consider the Bregman score (Parry et al., 2012) as follows*

$$s(p, p^*|x) = \sum_{k=1}^K \left\{[p^*(y_k|x) - p(y_k|x)]\,\psi'(p^*(y_k|x)) - \psi(p^*(y_k|x))\right\},$$

where ψ is a strictly concave and differentiable function. Bregman score reduces to the log score when $\psi(p) = p\log(p)$, and reduces to the Brier score when $\psi(p) = p^2 - \frac{1}{K}$.

So, let consider the strictly proper scoring rules $S(\mathbb{P}(Y|X), \mathbb{P}^*(Y|X))$ (Gneiting & Raftery, 2007; Bröcker, 2009), since $\mathbb{P}(Y|X)$ is predictive, and $\mathbb{P}^*(Y|X)$ is the data-generation distribution, then for $\mathcal{X}_{ood} = \mathcal{X}/\mathcal{X}_{idd}$, using the result from Liu et al. (2020a), we have

$$S(\mathbb{P}, \mathbb{P}^*) = \mathbb{E}_{x\sim X}(s(p, p^*|x)) = \int_{\mathcal{X}} s(p, p^*|x)p^*(x)dx \tag{16}$$

$$= \int_{\mathcal{X}} s(p, p^*|x)\left[p^*(x|x\in\mathcal{X}_{iid})p^*(x\in\mathcal{X}_{iid}) + p^*(x|x\in\mathcal{X}_{ood})p^*(x\in\mathcal{X}_{ood})\right]dx \tag{17}$$

$$= \underbrace{\mathbb{E}_{x\sim X_{iid}}(s(p, p^*|x))}_{S_{iid}(\mathbb{P},\mathbb{P}^*)} p^*(x\in\mathcal{X}_{iid}) + \underbrace{\mathbb{E}_{x\sim X_{ood}}(s(p, p^*|x))}_{S_{ood}(\mathbb{P},\mathbb{P}^*)} p^*(x\in\mathcal{X}_{ood}). \tag{18}$$

Therefore, since $S_{iid}(\mathbb{P}, \mathbb{P}^*)$ and $S_{ood}(\mathbb{P}, \mathbb{P}^*)$ has disjoint support, we have the minimax uncertainty risk, i.e., $\inf_{\mathbb{P}(Y|X)\in\mathcal{P}}\left[\sup_{\mathbb{P}^*(Y|X)\in\mathcal{P}_*} S(\mathbb{P}(Y|X), \mathbb{P}^*(Y|X))\right]$ equivalents to

$$\inf_{\mathbb{P}}\sup_{\mathbb{P}^*} S(\mathbb{P}, \mathbb{P}^*) = \inf_{\mathbb{P}}\left[\sup_{\mathbb{P}^*}[S_{iid}(\mathbb{P}, \mathbb{P}^*)]\cdot\mathbb{P}^*(X_{iid}) + \sup_{\mathbb{P}^*}[S_{ood}(\mathbb{P}, \mathbb{P}^*)]\cdot\mathbb{P}^*(X_{ood})\right] \tag{19}$$

$$= \inf_{\mathbb{P}}\sup_{\mathbb{P}^*}[S_{iid}(\mathbb{P}, \mathbb{P}^*)]\cdot\mathbb{P}^*(X_{iid}) + \inf_{\mathbb{P}}\sup_{\mathbb{P}^*}[S_{ood}(\mathbb{P}, \mathbb{P}^*)]\cdot\mathbb{P}^*(X_{ood}). \tag{20}$$

Due to $\mathbb{P}(Y|X_{iid})$ is the predictive distribution learned from data, we obtain $\inf_{\mathbb{P}} \sup_{\mathbb{P}^*} [S_{iid}(\mathbb{P}, \mathbb{P}^*)]$ is fixed and Density-Softmax satisfy by it is the model's predictive distribution learned from IID data. On the other hand, we have

$$\sup_{\mathbb{P}^* \in \mathcal{P}^*} [S_{ood}(\mathbb{P}, \mathbb{P}^*)] = \mathbb{E}_{x \sim X_{ood}} \sup_{p^*} [s(p, p^*|x)]\, p(x). \tag{21}$$

Applying the result from Lemma A.1 and combining with the result for OOD data from Theorem 4.4 and Proof A.1, we obtain

$$\sigma(p(f(x_{ood}); \alpha) \cdot g(f(x_{ood})) = \mathbb{U} = \arg\inf_{\mathbb{P} \in \mathcal{P}} \sup_{\mathbb{P}^* \in \mathcal{P}^*} [S_{ood}(\mathbb{P}, \mathbb{P}^*)]\,. \tag{22}$$

As a consequence, we obtain the conclusion: Density-Softmax's prediction is the optimal solution of the minimax uncertainty risk, i.e,

$$\sigma(p(f(X); \alpha) \cdot g(f(X)) = \arg\inf_{\mathbb{P}(Y|X) \in \mathcal{P}} \left[\sup_{\mathbb{P}^*(Y|X) \in \mathcal{P}*} S(\mathbb{P}(Y|X), \mathbb{P}^*(Y|X)) \right] \tag{23}$$

of Theorem 4.5. □

A.3. Proof of Theorem 4.6

Proof. The proof contains three parts. The first part shows density function $p(z_t; \alpha)$ is monotonically decreasing w.r.t. distance function $\mathbb{E} \|z_t - Z_s\|_{\mathcal{Z}}$. The second part shows the metric $u(x_t)$ is maximized if $p(z_t; \alpha) \to 0$. The third part shows $u(x_t)$ monotonically decreasing w.r.t. $p(z_t; \alpha)$ on the interval $(0, 1]$.

Part (1). The monotonic decrease of density function $p(z_t; \alpha)$ w.r.t. distance function $\mathbb{E} \|z_t - Z_s\|_{\mathcal{Z}}$: Consider the probability density function $p(z_t; \alpha)$ follows Normalizing-Flows which output the Gaussian distribution with mean (median) μ and standard deviation σ, then we have

$$p(z_t; \alpha) = \frac{1}{\sigma\sqrt{2\pi}} \exp\left(\frac{-1}{2} \left(\frac{z_t - \mu}{\sigma} \right)^2 \right). \tag{24}$$

Take derivative, we obtain

$$\frac{d}{dz_t} p(z_t; \alpha) = \left[\frac{-1}{2} \left(\frac{z_t - \mu}{\sigma} \right)^2 \right]' p(z_t; \alpha) = \frac{\mu - z_t}{\sigma^2} p(z_t; \alpha) \Rightarrow \begin{cases} \frac{d}{dz_t} p(z_t; \alpha) > 0 & \text{if } z_t < \mu, \\ \frac{d}{dz_t} p(z_t; \alpha) = 0 & \text{if } z_t = \mu, \\ \frac{d}{dz_t} p(z_t; \alpha) < 0 & \text{if } z_t > \mu. \end{cases} \tag{25}$$

Consider the distance function $\mathbb{E} \|z_t - Z_s\|_{\mathcal{Z}}$ follows the absolute norm, then we have

$$\mathbb{E} \|z_t - Z_s\|_{\mathcal{Z}} = \mathbb{E} (|z_t - Z_s|) = \int_{-\infty}^{z_t} \mathbb{P}(Z_s \le t) dt + \int_{z_t}^{+\infty} \mathbb{P}(Z_s \ge t) dt. \tag{26}$$

Take derivative, we obtain

$$\frac{d}{dz_t} \mathbb{E} \|z_t - Z_s\|_{\mathcal{Z}} = \mathbb{P}(Z_s \le z_t) - \mathbb{P}(Z_s \ge z_t) \Rightarrow \begin{cases} \frac{d}{dz_t} \mathbb{E} \|z_t - Z_s\|_{\mathcal{Z}} < 0 & \text{if } z_t < \mu, \\ \frac{d}{dz_t} \mathbb{E} \|z_t - Z_s\|_{\mathcal{Z}} = 0 & \text{if } z_t = \mu, \\ \frac{d}{dz_t} \mathbb{E} \|z_t - Z_s\|_{\mathcal{Z}} > 0 & \text{if } z_t > \mu. \end{cases} \tag{27}$$

Combining the result in Eq. 25 and Eq. 27, we have $p(z_t;\alpha)$ is maximized when $\mathbb{E}\left\|z_t - Z_s\right\|_{\mathcal{Z}}$ is minimized at the median μ, $p(z_t;\alpha)$ increase when $\mathbb{E}\left\|z_t - Z_s\right\|_{\mathcal{Z}}$ decrease and vice versa. As a consequence, we obtain $p(z_t;\alpha)$ is monotonically decreasing w.r.t. distance function $\mathbb{E}\left\|z_t - Z_s\right\|_{\mathcal{Z}}$.

Part (2). The maximum of metric $u(x_t)$: Consider $u(x_t) = v(d(x_t, X_s))$ in Def. 4.2, let $u(x_t)$ is the entropy of predictive distribution of Density-Softmax $\sigma(p(z = f(x);\alpha)\cdot(g\circ f(x)))$, then we have

$$u(x_t) = \mathrm{H}(\sigma(p(z_t;\alpha)\cdot g(z_t))) \tag{28}$$

$$= -\sum_{i=1}^{K} p(y=i|\sigma(p(z_t;\alpha)\cdot g(z_t)))\log\left(p(y=i|\sigma(p(z_t;\alpha)\cdot g(z_t)))\right) \tag{29}$$

$$= -\sum_{i=1}^{K} \frac{\exp(p(z_t;\alpha)\cdot(z_t^\top\theta_{g_i}))}{\sum_{j=1}^{K}\exp(p(z_t;\alpha)\cdot(z_t^\top\theta_{g_j}))}\log\left(\frac{\exp(p(z_t;\alpha)\cdot(z_t^\top\theta_{g_i}))}{\sum_{j=1}^{K}\exp(p(z_t;\alpha)\cdot(z_t^\top\theta_{g_j}))}\right). \tag{30}$$

Let $a_i = \frac{\exp(p(z_t;\alpha)\cdot(z_t^\top\theta_{g_i}))}{\sum_{j=1}^{K}\exp(p(z_t;\alpha)\cdot(z_t^\top\theta_{g_j}))}$, then we need to find

$$(a_1,\ldots,a_K) \text{ to maximize } -\sum_{i=1}^{K}(a_i)\log(a_i) \text{ subject to } \sum_{i=1}^{K}(a_i) - 1 = 0. \tag{31}$$

Since $-\sum_{i=1}^{K}(a_i)\log(a_i)$ is an entropy function, it strictly concave on $\vec{a}$. In addition, because the constraint is $\sum_{i=1}^{K}(a_i) - 1 = 0$, the Mangasarian-Fromovitz constraint qualification holds. So, apply the Lagrange multiplier, we have the Lagrange function

$$\mathcal{L}(a_1,\ldots,a_K,\lambda) = -\sum_{i=1}^{K}(a_i)\log(a_i) - \lambda\left(\sum_{i=1}^{K}(a_i) - 1\right). \tag{32}$$

Calculate the gradient, and we obtain

$$\nabla_{a_1,\ldots,a_K,\lambda}\mathcal{L}(a_1,\ldots,a_K,\lambda) = \left(\frac{\partial\mathcal{L}}{\partial a_1},\ldots,\frac{\partial\mathcal{L}}{\partial a_K},\frac{\partial\mathcal{L}}{\partial\lambda}\right) \tag{33}$$

$$= \left(-(\log(a_1)+\frac{1}{\ln}) - \lambda,\ldots,-(\log(a_k)+\frac{1}{\ln}) - \lambda, \sum_{i=1}^{K}(a_i) - 1\right), \tag{34}$$

and therefore

$$\nabla_{a_1,\ldots,a_K,\lambda}\mathcal{L}(a_1,\ldots,a_K,\lambda) = 0 \Leftrightarrow \begin{cases} -(\log(a_i)+\frac{1}{\ln}) - \lambda = 0, \forall i\in\mathcal{Y}, \\ \sum_{i=1}^{K}(a_i) - 1 = 0. \end{cases} \tag{35}$$

Consider $-(\log(a_i)+\frac{1}{\ln}) - \lambda = 0, \forall i\in\mathcal{Y}$, this shows that all a_i are equal (because they depend on λ only). By using $\sum_{i=1}^{K}(a_i) - 1 = 0$, we find

$$a_i = \frac{\exp(p(z_t;\alpha)\cdot(z_t^\top\theta_{g_i}))}{\sum_{j=1}^{K}\exp(p(z_t;\alpha)\cdot(z_t^\top\theta_{g_j}))} = \frac{1}{K}, \forall i\in\mathcal{Y}. \tag{36}$$

As a consequence, $u(x_t)$ is maximized if the predictive distribution $\sigma(p(z = f(x);\alpha)\cdot(g\circ f(x))) = \mathbb{U}$, i.e., $p(z_t;\alpha)\to 0$ which will happen if z_t is OOD data (by the result in Thm. 4.4 and Proof A.1).

Part (3). The monotonically decrease of metric $u(x_t)$ on the interval $(0,1]$: Consider the function

$$\mathcal{F}(p(z_t;\alpha)) = -\sum_{i=1}^{K} \frac{\exp(p(z_t;\alpha)\cdot(z_t^\top\theta_{g_i}))}{\sum_{j=1}^{K}\exp(p(z_t;\alpha)\cdot(z_t^\top\theta_{g_j}))}\log\left(\frac{\exp(p(z_t;\alpha)\cdot(z_t^\top\theta_{g_i}))}{\sum_{j=1}^{K}\exp(p(z_t;\alpha)\cdot(z_t^\top\theta_{g_j}))}\right). \tag{37}$$

Let $a = p(z_t;\alpha)$, $b_i = z_t^\top \theta_{g_i}, \forall i \in \mathcal{Y}$ then $\mathcal{F}(a) = -\sum_{i=1}^K \frac{e^{ab_i}}{\sum_{j=1}^K e^{ab_j}} \log\left(\frac{e^{ab_i}}{\sum_{j=1}^K e^{ab_j}}\right)$, and we need to find $\frac{d}{da}\mathcal{F}$. Take derivative, we obtain

$$\frac{d}{da}\mathcal{F} = -\sum_{i=1}^K \left\{ \left(\frac{e^{ab_i}}{\sum_{j=1}^K e^{ab_j}}\right)' \log\left(\frac{e^{ab_i}}{\sum_{j=1}^K e^{ab_j}}\right) + \frac{e^{ab_i}}{\sum_{j=1}^K e^{ab_j}} \left[\log\left(\frac{e^{ab_i}}{\sum_{j=1}^K e^{ab_j}}\right)\right]' \right\} \tag{38}$$

$$= -\sum_{i=1}^K \left[\left(\frac{e^{ab_i}}{\sum_{j=1}^K e^{ab_j}}\right)' \log\left(\frac{e^{ab_i}}{\sum_{j=1}^K e^{ab_j}}\right) + \frac{e^{ab_i}}{\sum_{j=1}^K e^{ab_j}} \left(\frac{e^{ab_i}}{\sum_{j=1}^K e^{ab_j}}\right)' \frac{\sum_{j=1}^K e^{ab_j}}{e^{ab_i}} \right] \tag{39}$$

$$= -\sum_{i=1}^K \left\{ \frac{b_i e^{ab_i}\sum_{j=1}^K e^{ab_j} - e^{ab_i}\sum_{j=1}^K b_j e^{ab_j}}{(\sum_{j=1}^K e^{ab_j})^2} \left[\log\left(\frac{e^{ab_i}}{\sum_{j=1}^K e^{ab_j}}\right) + 1\right] \right\} \tag{40}$$

$$= -\sum_{i=1}^K \left\{ \frac{\sum_{j=1}^K e^{a(b_i+b_j)}(b_i - b_j)}{(\sum_{j=1}^K e^{ab_j})^2} \left[\log\left(\frac{e^{ab_i}}{\sum_{j=1}^K e^{ab_j}}\right) + 1\right] \right\}. \tag{41}$$

By assuming the non-uniform in the predictive distribution $\sigma(g(f(x_{ood}))) \neq \mathbb{U}$ and $a \in (0, 1]$, then

$$\frac{d}{da}\mathcal{F} = -\sum_{i=1}^K \left\{ \frac{\sum_{j=1}^K e^{a(b_i+b_j)}(b_i - b_j)}{(\sum_{j=1}^K e^{ab_j})^2} \left[\log\left(\frac{e^{ab_i}}{\sum_{j=1}^K e^{ab_j}}\right) + 1\right] \right\} < 0, \tag{42}$$

combining with $u(x_t)$ is maximized if $a \to 0$, we obtain $u(x_t)$ decrease monotonically on the interval $(0, 1]$.

Combining the result in *Part (2).* $u(x_t)$ is maximized if $p(z_t;\alpha) \to 0$ which will happen if z_t is OOD data, and the result in *Part (3).* $u(x_t)$ is decrease monotonically w.r.t. $p(z_t;\alpha)$ on the interval $(0, 1]$ which will happen if x_t is closer to IID data since the likelihood value $p(z_t;\alpha)$ increases, we obtain the distance awareness of $p(z = f(x);\alpha) \cdot g$.

Combining the result in *Part (1).* $p(z_t;\alpha)$ is monotonically decreasing w.r.t. distance function $\mathbb{E}\left\|z_t - Z_s\right\|_{\mathcal{Z}}$ and the result *distance awareness* of $p(z = f(x);\alpha) \cdot g$, we obtain the conclusion: $\sigma(p(z = f(x);\alpha) \cdot (g \circ f(x)))$ is distance aware on latent space $\mathcal{Z}$ of Theorem 4.6. □

A.4. Proof of Proposition 4.8

Proof. Let us consider the prediction of the standard softmax $\sigma(g(f(x)))$. By definition, we have

$$\sigma: \quad \mathbb{R}^K \to \Delta_y \tag{43}$$

$$g(f(x)) \mapsto \sigma(g(f(x))). \tag{44}$$

Let the logit vectors of $g(f(x))$ be $u = (u_1, \cdots, u_K) \in \mathbb{R}^K$, for an arbitrary pair of classes, i.e., $\forall i, j \in \{1, \cdots, K\}$ of the logit vector u, assume that $u_i < u_j$. Since the predictive distribution of Desnity-Softmax is $\sigma(p(f(x);\alpha) \cdot g(f(x)))$, we have the corresponding logit vector is

$$p(f(x);\alpha) \cdot u = (p(f(x);\alpha) \cdot u_1, \cdots, p(f(x);\alpha) \cdot u_K) \in \mathbb{R}^K. \tag{45}$$

Due to $p(f(x);\alpha) \in (0, 1]$, then we obtain the following relationship holds

$$[p(f(x);\alpha) \cdot u]_i < [p(f(x);\alpha) \cdot u]_j, \tag{46}$$

where $[\cdot]_i$ represents the i-th entry of the vector. Since the order of entries in the logit vector is unchanged between the standard softmax and Density-Softmax, we obtain

$$\arg\max_{y \in \mathcal{Y}} [\sigma(g(f(x)))]_y = \arg\max_{y \in \mathcal{Y}} [\sigma(p(f(x);\alpha) \cdot g(f(x))]_y. \tag{47}$$

As a consequence, Density-Softmax preserves the accuracy of the standard softmax by

$$\text{acc}(B_m) = \frac{1}{|B_m|}\sum_{i\in B_m}\mathbb{I}(\arg\max_{y\in\mathcal{Y}}[\sigma(g(f(x_i)))]_y = y_i) \tag{48}$$

$$= \frac{1}{|B_m|}\sum_{i\in B_m}\mathbb{I}(\arg\max_{y\in\mathcal{Y}}[\sigma(p(f(x_i);\alpha)\cdot g(f(x_i)))]_y = y_i), \tag{49}$$

where B_m is the set of sample indices whose confidence falls into $\left(\frac{m-1}{M}, \frac{m}{M}\right]$ in M bins.

On the other hand, since $p(f(x);\alpha) \in (0, 1]$, we also have

$$\max_{y\in\mathcal{Y}}\left[\sigma(p(f(x);\alpha)\cdot g(f(x)))\right]_y \leq \max_{y\in\mathcal{Y}}[\sigma(g(f(x)))]_y, \tag{50}$$

and this yields

$$\frac{1}{|B_m|}\sum_{i\in B_m}\max_{y\in\mathcal{Y}}[\sigma(p(f(x_i);\alpha)\cdot g(f(x_i)))]_y \leq \frac{1}{|B_m|}\sum_{i\in B_m}\max_{y\in\mathcal{Y}}[\sigma(g(f(x_i)))]_y. \tag{51}$$

Furthermore, by assuming the predictive distribution of the standard softmax layer $\sigma(g(f(x)))$ is over-confident, i.e., $\text{acc}(B_m) \leq \text{conf}(B_m), \forall B_m$, then we have

$$0 \leq \frac{1}{|B_m|}\sum_{i\in B_m}\mathbb{I}(\arg\max_{y\in\mathcal{Y}}[\sigma(g(z_i))]_y = y_i) \leq \frac{1}{|B_m|}\sum_{i\in B_m}\max_{y\in\mathcal{Y}}[\sigma(g(z_i))]_y, \forall B_m. \tag{52}$$

Combining with the result in 48, in 51 and in 51 together, for N number of samples, we obtain

$$\underbrace{\sum_{m=1}^{M}\frac{|B_m|}{N}\left|\frac{1}{|B_m|}\sum_{i\in B_m}\mathbb{I}(\arg\max_{y\in\mathcal{Y}}[\sigma(p(z_i;\alpha)\cdot g(z_i))]_y = y_i) - \frac{1}{|B_m|}\sum_{i\in B_m}\max_{y\in\mathcal{Y}}[\sigma(p(z_i;\alpha)\cdot g(z_i))]_y\right|}_{\text{ECE}(\sigma((p(f;\alpha)\cdot g)\circ f))} \tag{53}$$

$$\leq \underbrace{\sum_{m=1}^{M}\frac{|B_m|}{N}\left|\frac{1}{|B_m|}\sum_{i\in B_m}\mathbb{I}(\arg\max_{y\in\mathcal{Y}}[\sigma(g(z_i))]_y = y_i) - \frac{1}{|B_m|}\sum_{i\in B_m}\max_{y\in\mathcal{Y}}[\sigma(g(z_i))]_y\right|}_{\text{ECE}(\sigma(g\circ f))}, \text{ where } z_i = f(x_i). \tag{54}$$

As a consequence, we obtain the conclusion: $\text{ECE}(\sigma((p(f;\alpha)\cdot g)\circ f) \leq \text{ECE}(\sigma(g\circ f))$ of Proposition 4.8. □

B. Further discussion and Ablation study

B.1. Density estimation and likelihood value

Recall that the output in the inference step of Algorithm 1 has the form

$$p(y = i|x_t) = \frac{\exp(p(z_t;\alpha)\cdot(z_t^\top\theta_{g_i}))}{\sum_{j=1}^{K}\exp(p(z_t;\alpha)\cdot(z_t^\top\theta_{g_j}))}, \forall i \in \mathcal{Y}. \tag{55}$$

Let's consider: $\exp(p(z_t;\alpha)\cdot(z_t^\top\theta_{g_i}))$, if the likelihood value of $p(z_t;\alpha)$ is too large, then the output of the exponential function may go to a very large value, leading to the computer can not store to compute. Therefore, we need to find a scaling technique to avoid this issue.

Recall that for density estimation, we use Normalizing-Flows (Dinh et al., 2017; Papamakarios et al., 2021). Instead of returning likelihood value $p(Z;\alpha)$, this estimation returns the logarithm of likelihood $\log(p(Z;\alpha))$, then we need to take exponentially to get the likelihood value by

$$p(Z;\alpha) = e^{\log(p(Z;\alpha))}. \tag{56}$$

Algorithm 2 Scaling likelihood

Scaling Input: Training data D_s, encoder f, trained density function $p(Z;\alpha)$.
max_trainNLL $\leftarrow 0$
for $e = 1 \rightarrow$ epochs **do**
  Sample D_B with a mini-batch B for source data D_s
  $Z = f(X \in D_B)$
  batch_trainNLL $\leftarrow p(Z;\alpha)$
  if $\max$(batch_trainNLL) $>$ max_trainNLL **then**
    max_trainNLL $\leftarrow \max$(batch_trainNLL)
  end if
end for
Scaling Inference Input: Test sample x_t
$z_t = f(x_t)$
$p(z_t;\alpha) = \frac{p(z_t;\alpha)}{\text{max\_trainNLL}}$

By doing so, there will be two properties for the range of likelihood value $p(Z;\alpha)$. First, value of $p(Z;\alpha) \neq 0$ by $\log(0)$ being undefined. Second, $p(Z;\alpha)$ is always positive by the output of the exponential function is always positive. As a result, we obtain the likelihood value $p(Z;\alpha)$ is in the range of $(0, +\infty]$.

To avoid the numerical issue when $p(Z;\alpha) \rightarrow +\infty$, we use the scaling technique to scale the range $(0, +\infty]$ to $(0, 1]$ by the following formula

$$p(Z;\alpha) = \frac{p(Z;\alpha)}{\max(p(Z_{train};\alpha))}. \tag{57}$$

It is also worth noticing that there also can be a case $e^{\log(p(Z;\alpha))}$ in Equation 56 goes to $+\infty$ if $\log(p(Z;\alpha))$ is too large, therefore, we also need to scale it to avoid the numerical issue. The pseudo-code of our scaling algorithm and inference process is presented in Algorithm 2.

B.2. Distance preserving and 1-Lipschitz constraint

To improve the uncertainty quality, Liu et al. (2020a) introduce distance awareness definition on sample space $\mathcal{X}$, which is stronger than our definition on feature space $\mathcal{Z}$. However, to make the model distance aware on $\mathcal{X}$, one necessary condition is $f(x)$ must be an isometric mapping, i.e., distance preserving on latent space $\mathcal{Z}$ by satisfy the bi-Lipschitz condition (Searcód, 2006)

$$L_1 \cdot \|x_1 - x_2\|_{\mathcal{X}} \leq \|f(x_1) - f(x_2)\|_{\mathcal{Z}} \leq L_2 \cdot \|x_1 - x_2\|_{\mathcal{X}}\,, \tag{58}$$

for positive and bounded constants $0 < L1 < 1 < L2$. Although our model only guarantees distance awareness on $\mathcal{Z}$ and does not hold on $\mathcal{X}$, it still aims to achieve the upper bound of Eq. 58 by the 1-Lipschitz constraint, i.e., $||f(x_1) - f(x_2)||_2 \leq ||x_1 - x_2||_2$. This helps $f(x)$ assure that if the sample is similar, the feature will be similar as well, providing meaningful correspondence with the semantic properties of the input data $\mathcal{X}$. Therefore, the 1-Lipschitz not only helps to improve robustness but may also support to improve uncertainty performance. The empirical evidence is confirmed in Table 5 by the calibrated uncertainty error without 1-Lipschitz constraint ($\lambda = 0$) is significantly higher than with 1-Lipschitz constraint (e.g., $\lambda = 1e-4$).

B.3. Additional ablation study: gradient-penalty and training cost

Tab. 5 shows the performance of Density-Softmax across different values of the gradient-penalty hyper-parameter λ. Firstly, we observe there is a trade-off between the performance on IID and OOD data w.r.t. λ, i.e., the Lipschitz constraint may affect model performance on IID and OOD data. Secondly, the fine-tuning classifier step in Eq. 6 is essential by a better performance of $\lambda = 1$ than $\lambda = 0$ (w/o Eq. 6). Finally, with an appropriate $\lambda = 1e-4$, Density-Softmax can balance the performance between IID and OOD data. Notably, this gradient-penalty not only helps to improve the accuracy but also the uncertainty by a lower ECE than $\lambda = 0$, confirming the hypothesis that the 1-Lipschitz constraint supports improving uncertainty quality at the same time.

λ	NLL(↓)	Acc(↑)	ECE(↓)	cNLL(↓)	cAcc(↑)	cECE(↓)
0	0.142	96.1	0.015	0.79	77.0	0.086
1 (w/o Eq. 6)	0.165	94.8	0.017	0.66	79.9	0.041
1	0.162	95.0	0.015	0.64	80.0	0.039
1e-1	0.159	95.2	0.014	0.66	79.3	0.040
1e-2	0.146	95.6	0.009	0.66	79.7	0.047
1e-3	0.144	95.7	0.012	0.66	79.9	0.051
1e-4	0.137	96.0	0.010	0.68	79.2	0.060

Table 5. Performance of Density-Softmax with different gradient-penalty coefficient λ, model is trained on CIFAR-10, tested on IID CIFAR-10 and OOD CIFAR-10-C.

Despite showing success in test-time efficiency, we raise awareness about the challenge of training Density-Softmax on low computational infrastructure. Specifically, Density-Softmax requires a longer-time and higher-memory cost than Deterministic ERM at training time (e.g., Fig. 6), due to 3 separate training steps and the Jacobian matrix in the regularization at the first step of Algorithm 1. This 1-Lipschitz regularization also requires pre-defining the hyper-parameter λ before training in implementation (e.g., Tab. 5). Additionally, the 3 training steps also require pre-defining additional optimizers, iterations, and learning rates in Tab. 6. That said, our training cost is still lower than other SOTA techniques, e.g., Deep Ensembles, BatchEnsemble, MIMO, Rank-1 BNN in Fig. 6 (left). Importantly, the efficient benefits of Density-Softmax are illustrated with a much lower inference cost than other SOTA methods at test time in Fig. 6 (right).

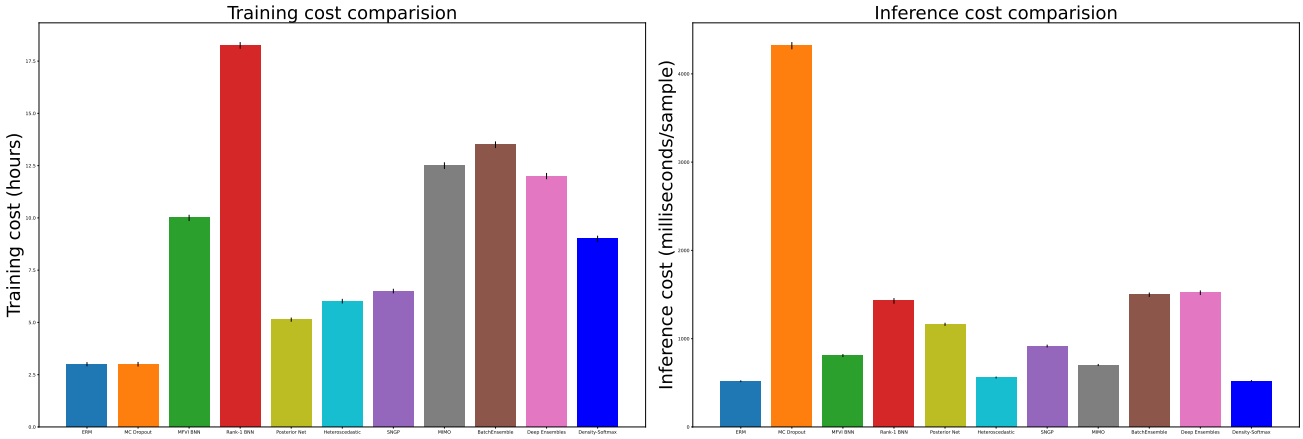

Figure 6. Comparison in training cost (hours) on NVIDIA A100 and inference cost (milliseconds/sample) on NVIDIA RTX A5000, with error bars across 10 seeds of Wide Resnet-28-10 on CIFAR-10 dataset. Density-Softmax outperforms SOTA in inference speed and still has a lower training cost than some baselines.

B.4. Additional discussion about our method

Lipschitz gradient penalty and the sufficient condition to 1-Lipschitz. Since the feature extractor f is a neural network, we can not verify whether f is a 1-Lipschitz. However, there are two observations we want to discuss. Firstly, we note that our feature extractor f satisfies $\sup_x ||\nabla_x f(x)||_2 = 1$ in training data with the Rademacher Theorem 3.1. Secondly, we tried the SeqLip (Virmaux & Scaman, 2018) to approximate the Lipschitz constant $L(f)$ by computing the upper bound of $L(f)$ with the Wide Renet 28-10 backbone on the CIFAR-10. We observe that the upper bounds of $L(f)$ are about $4.5 \cdot 10^6$ without gradient-penalty and $2.8 \cdot 10^6$ with gradient-penalty regularization. This does not show whether our true $L(f)$ is equal to 1 or not, but at least, it shows the gradient-penalty regularization can reduce the upper bound of $L(f)$.

Potential to use with pre-trained large models. Although we train the backbone from scratch, our method is flexible to be used to improve the uncertainty of a pre-trained model. Specifically, our training of the density function in Eq. 5 and our update classifier weight in Eq. 6 do not require backpropagation through the feature backbone f. Therefore, we can use these two training steps to fine-tune a pre-trained model to enhance uncertainty estimation, like Vision Transformer (Dosovitskiy et al., 2021). We also show this improvement in Tab. 5, with $\lambda = 0$, our method achieves 0.015 in ECE and 0.086 in cECE, while the pre-trained model, i.e., Deterministic ERM only achieves 0.023 in ECE and 0.053 in cECE in Tab. 2.

Comparison with OOD detection related work. Our method aims to improve calibration (both empirical and theoretical analysis of the calibration level w.r.t. ECE in Prop. 4.8) but also can be used for OOD detection in Sec. 5, while OOD detection methods (Dosovitskiy et al., 2021; Lee et al., 2018b; Sun et al., 2022), in contrast, are not explicitly designed to improve calibration. Regarding test-time efficiency, these methods also suffer from a heavy computational burden. In particular, Lee et al. (2018b) calculates expensive invertible covariance matrixes whose size depends on the feature dimension and the class number for multiple DNN layers, additionally the cost of the derivative w.r.t. the input sample. Meanwhile, Dosovitskiy et al. (2021); Sun et al. (2022) are non-parametric methods whose computational complexity at test-time depends on the number of training samples. In contrast, our model estimates a marginal lightweight density function and is a parametric method, hence, the complexity at test-time does not depend on the size of the training set.

C. Additional experiments

C.1. Baseline details

This appendix provides an exhaustive literature review of 14 SOTA related methods which are used to make comparisons with our model by using the uncertainty-baselines (Nado et al., 2021) (We exclude Mixup (Zhang et al., 2018; Carratino et al., 2022) and Augmix (Hendrycks* et al., 2020) by we do not use data-augmentation):

- **Deterministic ERM (Vapnik, 1998)** is a standard deterministic model. In test time, it predicts the label immediately by a single forward pass.
- **MC Dropout (Gal & Ghahramani, 2016b)** includes dropout regularization method in the model. In test time, it uses MC sampling by dropout to make different predictions, then get the mean of the list prediction.
- **MFVI BNN (Wen et al., 2018)** uses the BNN by putting distribution over the weight by mean and variance per each weight. Because each weight consists of mean and variance, the total model weights will double as the Deterministic ERM model.
- **Rank-1 BNN (Dusenberry et al., 2020)** use the mixture approximate posterior to benefits from multimodal representation with local uncertainty around each mode, compute posterior on rank-1 matrix while keeping weight is deterministic. In inference time, sampling weight distribution by MC to make different predictions, then get the mean of the list prediction.
- **Posterior Net (Charpentier et al., 2020)** is based on Evidential Deep Learning (Sensoy et al., 2018) with a latent density function by utilizing conditional densities per class, intuitively acting as class conditionals on the latent space. Due to belonging to the Bayesian perspective, it needs to select a "good" Prior distribution, which is difficult in practice.
- **Heteroscedastic (Collier et al., 2021)** is a probabilistic approach to modeling input-dependent by placing a multivariate Normal distributed latent variable on the final hidden layer of a neural network classifier. In test time, it uses MC sampling to make different predictions, then get the mean of the list prediction.
- **SNGP (Liu et al., 2020a)** is a combination of the last Gaussian Process layer with Spectral Normalization to the hidden layers. Because using the Spectral Normalization for every weight in each residual layer with the power iteration method (Gouk et al., 2021; Miyato et al., 2018), and Gaussian Process layer with MC sampling, the weight and latency of SNGP is considerably higher than the Deterministic ERM model.
- **MIMO** (Havasi et al., 2021), i.e., multi-input multi-output, it trains multiple independent subnetworks within a network. In test time, it performs multiple independent predictions in a single forward pass.
- **DUQ (Van Amersfoort et al., 2020)** is a deterministic-based framework by using kernel distance with Radial Basis Function to improve OOD detection ability. However, it has been shown often to have a poor performance in uncertainty and robustness (Liu et al., 2020a; Nado et al., 2021). Regarding scalability, this requires storing and computing a weight matrix with the size depending quadratically on latent dimension and linearly in the number of classes, leading to high computational demands across modern DNN architectures at inference time.
- **DDU (Mukhoti et al., 2023)** is another deterministic-based method, which is a combination of ERM with a Gaussian Mixture Models (GMM) density function to detect OOD samples. However, this OOD detector does not contribute to the predictive distribution of the softmax directly. As a result, this method needs to apply the post-hoc re-calibration

technique to improve calibration performance. Meanwhile, we focus on methods that do not require additional calibration data and post-hoc calibration steps, i.e., without Temperature Scaling (w/o TS).

- **DUE (van Amersfoort et al., 2022)** is an extension version of SNGP by constrain Deep Kernel Learning's feature extractor to approximately preserve distances through a bi-Lipschitz constraint.
- **NatPN (Charpentier et al., 2022)** is based on Posterior Net and is the closest to our work by also estimating the density function on the marginal feature space. Yet, we have two main differences: (1) From the Bayesian view, optimizing with NatPN is equivalent to doing Maximum a Posteriori estimation while ours is equivalent to doing MLE. (2) The predictive distribution in NatPN is not a standard softmax output because it is not normalized by a natural exponent function. Meanwhile, Density-Softmax is normalized by a natural exponent function. So, we have the following benefits: (1) Density-Softmax can calculate the predictive distribution without the need to consider how to define prior parameters. The prior can hurt the posterior performance in NatPN if we pre-define a bad prior. (2) The natural exponential helps Density-Softmax easily optimize with the cross-entropy loss by the nice derivative property of $\ln(\exp(a)) = a$ (Goodfellow et al., 2016), and produce a sharper distribution with a higher probability of the largest entry in the logit vector and lower probabilities of the smaller entries when compared with the normalization of NatPN.
- **BatchEnsemble (Wen et al., 2020)** defines each weight matrix to be the Hadamard product of a shared weight among ensemble members and a rank-1 matrix per member. In test time, the final prediction is calculated from the mean of the list prediction of the ensemble.
- **Deep Ensembles (Lakshminarayanan et al., 2017)** includes multiple Deterministic ERM trained with different seeds. In test time, the final prediction is calculated from the mean of the list ensemble predictions. Due to aggregates from multiple models, the total of model weights needed to store will increase linearly w.r.t. the number of models.

C.2. Implementation details

Based on the code of Nado et al. (2021), we use similar settings with their Deterministic ERM for everything for a fair comparison on the benchmark dataset. For the setting on the toy dataset, we follow the settings of Liu et al. (2020a).

Datasets. We utilize 6 commonly used datasets under distributional shifts (Nado et al., 2021), including Toy dataset (Liu et al., 2020a) with two moons and two ovals to visualize uncertainty and clustering. CIFAR-10-C, CIFAR-100-C, and ImageNet-C (Hendrycks & Dietterich, 2019) for the main benchmarking. To evaluate real-world shifts, we experiment on SVHN (Netzer et al., 2011) and CIFAR-10.1 (Recht et al., 2018).

Evaluation metrics. To evaluate the generalization, we use NLL and Accuracy. For uncertainty estimation, we visualize uncertainty surfaces (entropy, different predictive variances), predictive entropy, AUPR/AUROC for OOD detection, and ECE with 15 bins for calibration. To compare the robustness under distributional shifts, we evaluate every OOD set in each dataset. To compare computational efficiency, we count the number of model parameters for storage requirements and measure latency in milliseconds per sample **at test time**.

Training details. We train models on the train set excluding data augmentation (Hendrycks* et al., 2020; Zhang et al., 2018), test on the original IID test, and aforementioned OOD sets. The performance is evaluated on backbones ResFFN-12-128 (Liu et al., 2020a) for the Toy, Wide Resnet-28-10 (Zagoruyko & Komodakis, 2016) for CIFAR-10-100, and Resnet-50 (He et al., 2016) for ImageNet. We only use normalization to process images for the benchmark datasets. Specifically, for CIFAR-10 and CIFAR-100, we normalize by the mean is $[0.4914, 0.4822, 0.4465]$ and standard deviation is $[0.2470, 0.2435, 0.2616]$. For ImageNet, we normalize by the mean is $[0.485, 0.456, 0.406]$ and standard deviation is $[0.229, 0.224, 0.225]$ (note that we do not perform augmentation techniques of Hendrycks* et al. (2020) and Zhang et al. (2018)).

Architectures and hyper-parameters. We list the detailed value of hyper-parameters used for each dataset in Table 6 and the architecture of Normalizing-Flows in Table 7. For a fair comparison with deterministic, we always use the same hyper-parameters as the Deterministic ERM.

Source code and computing system. Our source code includes the notebook demo on the toy dataset, scripts to download the benchmark dataset, setup for environment configuration, and our provided code (detail in README.md). We train our model on two single GPUs: NVIDIA A100-PCIE-40GB with 8 CPUs: Intel(R) Xeon(R) Gold 6248R CPU @ 3.00GHz with 8GB RAM per each, and require 100GB available disk space for storage. We test our model on three different settings, including (1) a single GPU: NVIDIA Tesla K80 accelerator-12GB GDDR5 VRAM with 8-CPUs: Intel(R) Xeon(R) Gold

6248R CPU @ 3.00GHz with 8GB RAM per each; (2) a single GPU: NVIDIA RTX A5000-24564MiB with 8-CPUs: AMD Ryzen Threadripper 3960X 24-Core with 8GB RAM per each; and (3) a single GPU: NVIDIA A100-PCIE-40GB with 8 CPUs: Intel(R) Xeon(R) Gold 6248R CPU @ 3.00GHz with 8GB RAM per each.

Demo notebook code for Algorithm 1

```
import tensorflow as tf

#Define a features extractor f.
encoder = tf.keras.Sequential([
        tf.keras.layers.Dense(100, activation = "relu"),
        tf.keras.layers.Dense(100, activation = "relu"),
])
#Define a classifier g.
classifier = tf.keras.layers.Dense(10)

#Define a tf step function to pre-train model w.r.t. Eq. 4.
@tf.function
def pre_train_step(x, y):
    with tf.GradientTape(persistent = True) as tape:
        tape.watch(x)
        features = encoder(x)
        logits = classifier(features)
        loss_value = tf.cast(loss_fn(y, logits), tf.float64)
        grad_norm = tf.sqrt(tf.reduce_sum(tape.batch_jacobian(features, x)**2, axis = [1, 2]))
        loss_value += (grad_lambda * tf.reduce_mean(((grad_norm - 1)**2)))

    list_weights = encoder.trainable_weights + classifier.trainable_weights
    grads = tape.gradient(loss_value, list_weights)
    optimizer.apply_gradients(zip(grads, list_weights))
    return loss_value

#Define a tf step function to re-update the classifier by feature density model w.r.t. Eq. 6.
@tf.function
def train_step(x, y, flow_model, train_likelihood_max):
    with tf.GradientTape() as tape:
        features = encoder(x)
        likelihood = tf.exp(flow_model.score_samples(features))
        likelihood = (tf.expand_dims(likelihood, 1))/(train_likelihood_max)
        logits = classifier(features) * tf.cast(likelihood, dtype=tf.float32)
        loss_value = loss_fn(y, logits)

    grads = tape.gradient(loss_value, classifier.trainable_weights)
    optimizer.apply_gradients(zip(grads, classifier.trainable_weights))
    return loss_value

#Define a tf step function to make inference w.r.t. Eq. 7.
@tf.function
def test_step(x, flow_model, train_likelihood_max):
    features = encoder(x)
    likelihood = tf.exp(flow_model.score_samples(features))
    likelihood = (tf.expand_dims(likelihood, 1))/(train_likelihood_max)
    logits = classifier(features) * tf.cast(likelihood, dtype=tf.float32)
    y_pred = tf.nn.softmax(logits)
    return y_pred
```

C.3. Empirical result details

C.3.1. Distance awareness on the toy dataset

Different uncertainty metrics. Figure 7 presents a comparison in terms of predictive entropy. Because of the over-confidence of Deterministic ERM, MC Dropout, Rank-1 BNN, and Ensemble which return $p(y|x) = 0$, theirs predictive entropy become undefined by $\log_2(p(y|x)) = \log_2(0)$ is undefined. As a result, we have a white background for these mentioned baselines, showing these methods are not able to be aware of the distance OOD dataset. For MC Dropout and Ensemble, since these two methods do not provide a convenient expression of the predictive variance of Bernoulli distribution, we also follow the work of Liu et al. (2020a) to plot their predictive uncertainty as the distance of the maximum predictive probability from 0.5 so that $u(x) \in [0, 1]$ in Figure 8. Although with different uncertainty metrics, Deterministic ERM, MC Dropout, Rank-1 BNN, and Ensemble still perform badly, showing truly unable to have the distance-aware ability.

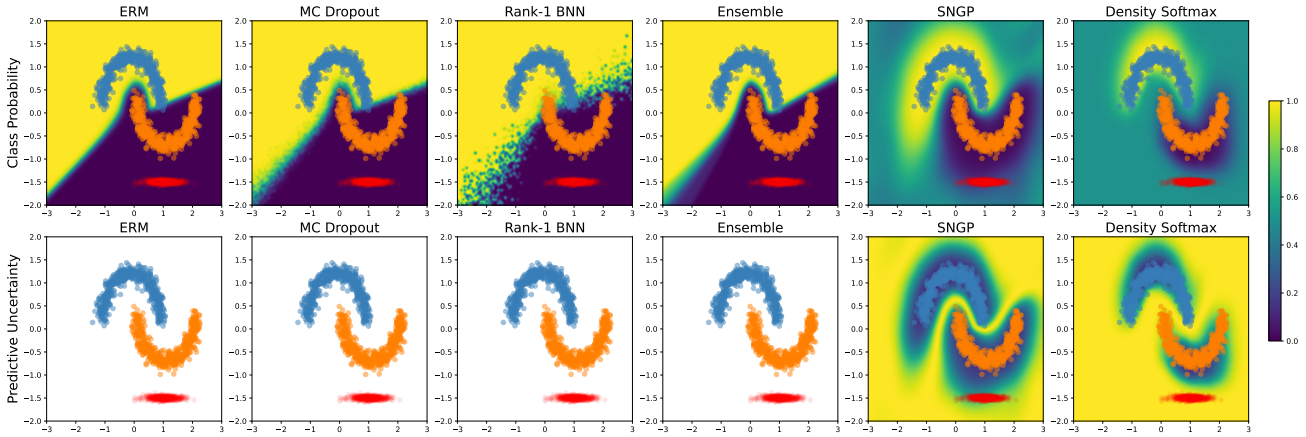

Figure 7. The class probability $p(y|x)$ (Top Row) and predictive entropy $H(Y|X = x) = -p(y|x) \cdot \log_2(p(y|x)) - (1 - p(y|x)) \cdot \log_2((1 - p(y|x)))$ surface (Bottom Row) between different approaches. Density-Softmax achieves distance awareness with a uniform class probability and high entropy value on OOD data. Note that the white background due to $\log(0)$ is undefined.

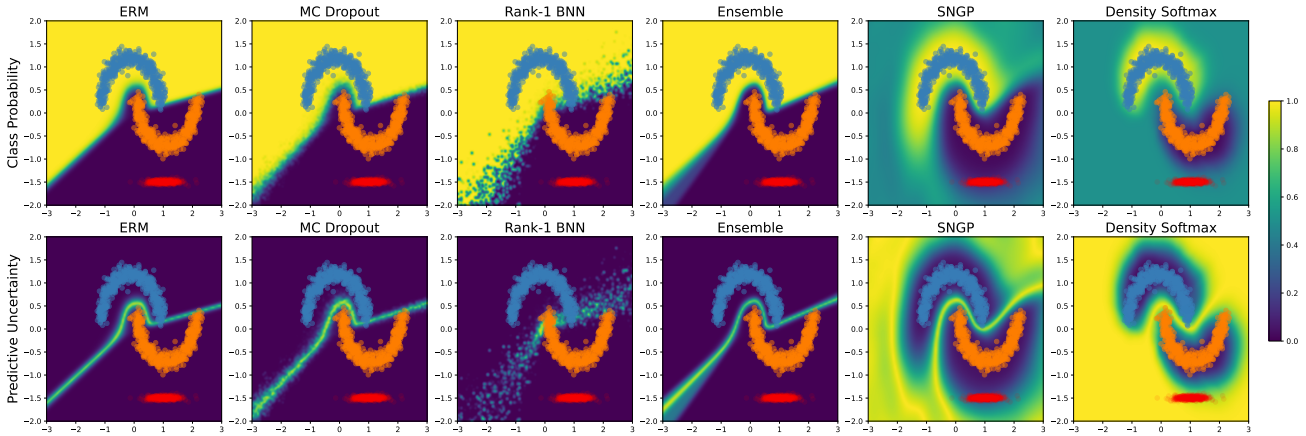

Figure 8. The class probability $p(y|x)$ and predictive uncertainty $u(x) = 1 - 2 \cdot |p(y|x) - 0.5|$ surface between different approaches.

Different toy dataset. To continue to verify a consistency observation across different empirical settings, we illustrate distance-aware ability by predictive variance surface on the second toy dataset. Figure 9 compares the methods as mentioned earlier on two ovals datasets. Similar to previous settings, only SNGP can show its distance-aware uncertainty. However, for around half of OOD data points, its predictive uncertainty is still 0.0, showing still has limitations in distance-aware ability. In contrast, our Density-Softmax performs well, with 0.0 uncertainty value on IID training data points while always returning 1.0 on OOD data points, confirming the hypothesis that our Density-Softmax is a better distance-aware method.

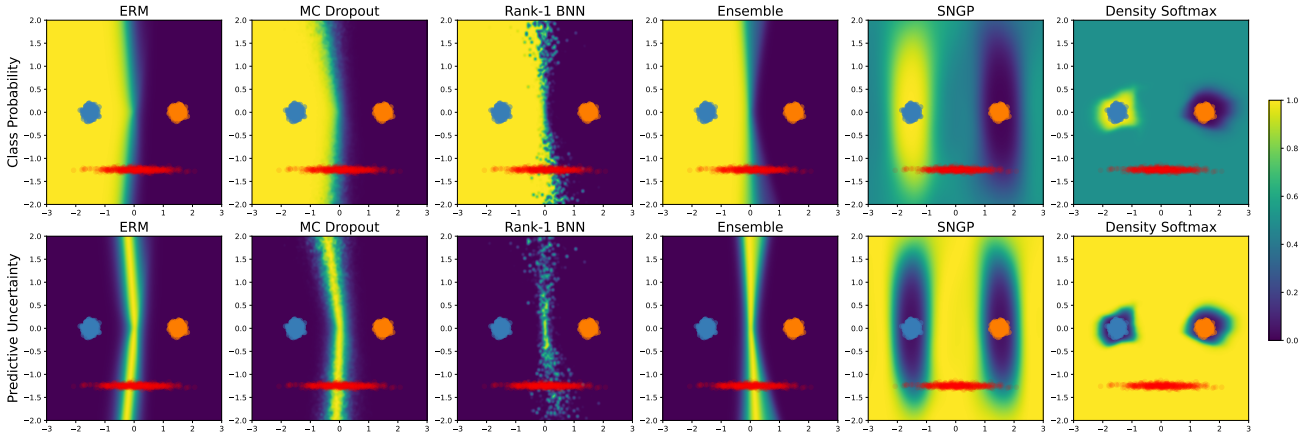

Figure 9. The class probability $p(y|x)$ and predictive uncertainty $u(x) = 1 - 2 \cdot |p(y|x) - 0.5|$ surface between different approaches on the two ovals 2D classification dataset.

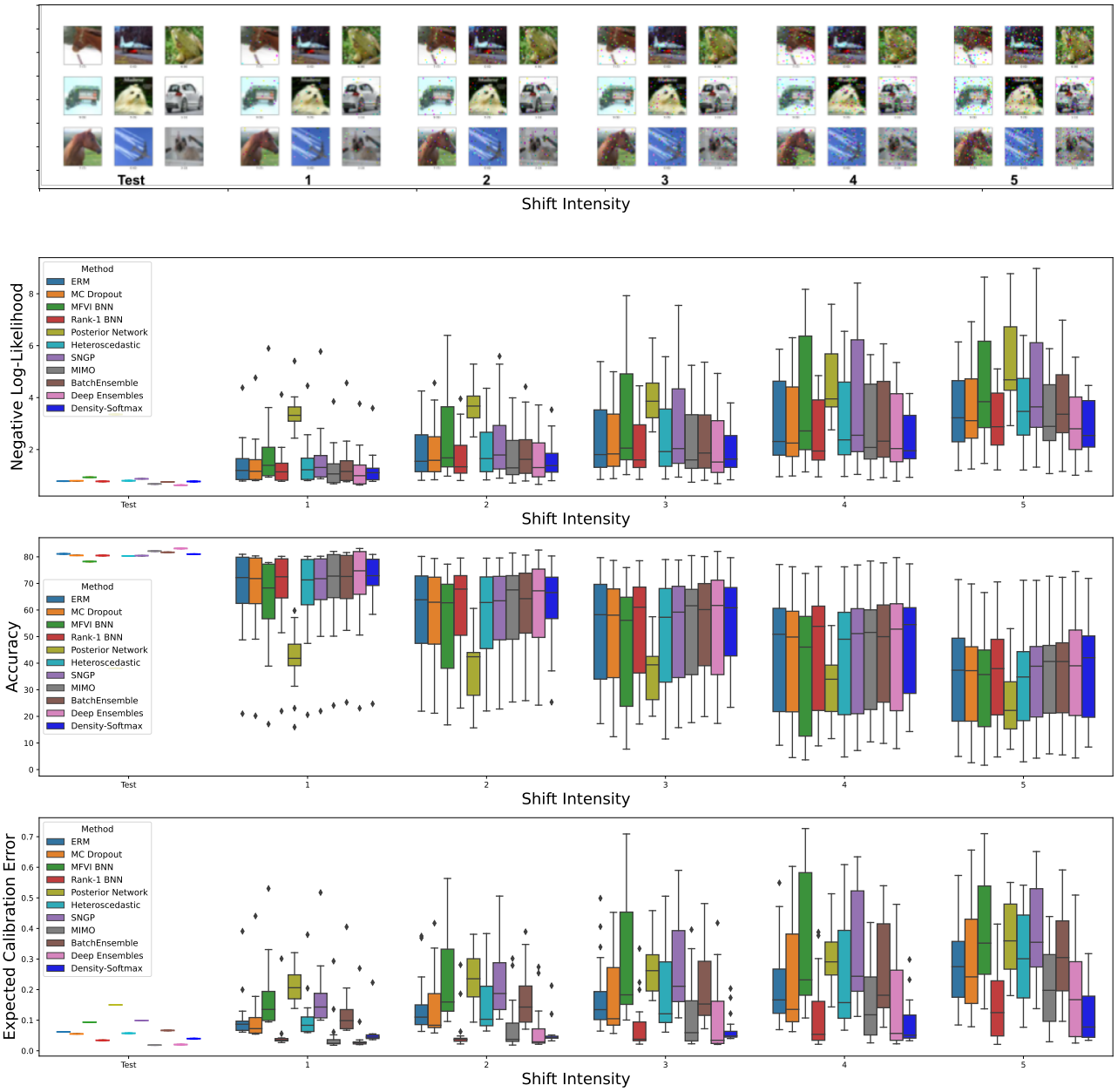

Figure 10. A corruption example by shift intensities and comparison under the distributional shift of negative log-likelihood, accuracy, and ECE under all types of corruptions in CIFAR-100-C. For each method, we show the mean on the test set and summarize the results on each shift intensity with a box plot. Each box shows the quartiles summarizing the results across all 17 types of shift while the error bars indicate the min and max across different shift types. Our Density-Softmax achieves the highest accuracy, lowest NLL and ECE with a low variance across different shift intensities.

C.3.2. Benchmark result details

To compare the uncertainty and robustness between methods in more detail, we visualize Figure 10, the box plots of the NLL, accuracy, and ECE across corruptions under distributional shifts level in CIFAR-100 based dataset from Table 3. Overall, besides achieving the highest accuracy, lowest NLL and ECE on average, our Density-Softmax also always achieves the best accuracy, NLL, and ECE performance across different shift intensities in Figure 10. For each intensity, our results also show a low variance, implying the stability of our algorithm across different corruption types. More importantly, compared to the two second-best methods Deep Ensembles and Rank-1 BNN, the gap between our methods increases when the level shift increases, showing our Density-Softmax is more robust than theirs under distributional shifts.

Figure 10 however only shows the statistics across different shift methods. Therefore, we next analyze in detail the above results over 10 different random seeds. Specifically, we train each model with a specific random seed and then evaluate the result. We repeatedly do this evaluation 10 times with 10 different seed values. Finally, collect 10 of these results together and visualize the mean and standard deviation by the error bar for each shift intensity level. Figure 11 shows these results in the CIFAR-10-C setting from Table 2, we observe that the result of our model and other baselines have a small variance, showing the consistency and stability across different random seeds.

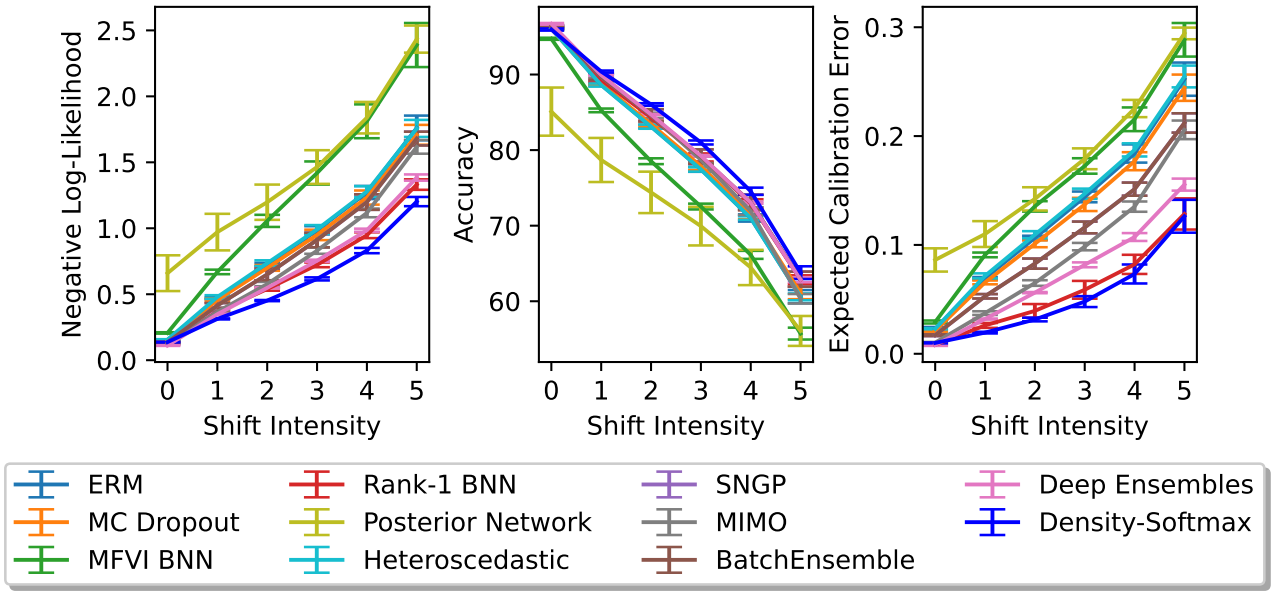

Figure 11. Benchmark performance on CIFAR-10-C with Wide Resnet-28-10 over 10 different random seeds. We plot NLL, accuracy, and ECE for varying corruption intensities; each result is the mean value over 10 runs and 15 corruption types. The error bars represent a fraction of the standard deviation across corruption types. Our method achieves competitive results with SOTA with low variance across different shift intensities.

Similarly, Figure 12 is the comparison across 10 running with 10 different random seeds in terms of model storage and inference cost from Table 2. There is no variance in storage comparison since the model size is fixed and not affected by a random seed. Meanwhile, the latency variances across different seeds are minor since narrow error bars are in the inference cost comparison bar chart. And this once again, confirms that the results are consistent and stable, our Density-Softmax is the fastest model with almost similar latency to a single Deterministic ERM.

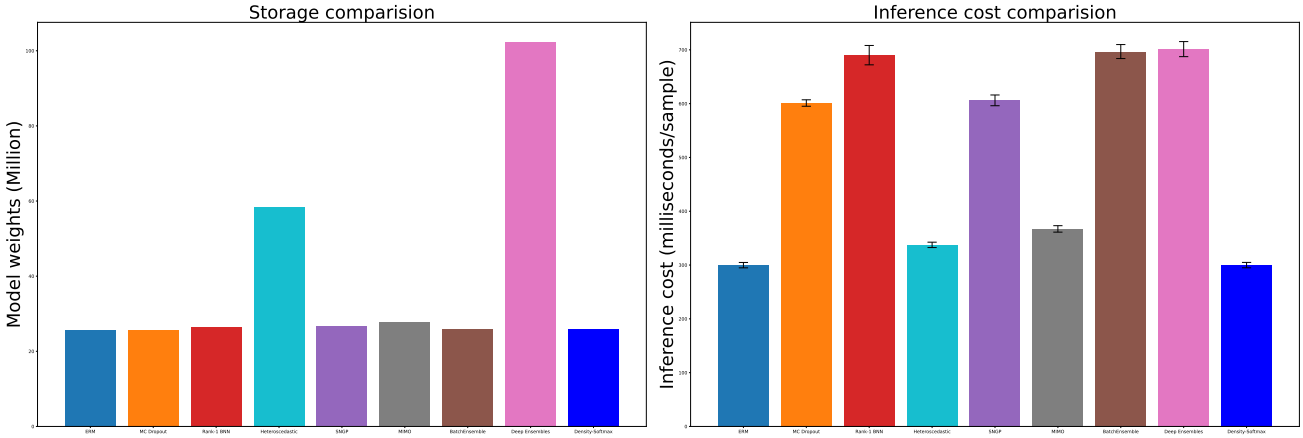

Figure 12. Comparison in model storage requirement (Million weights) and inference cost (milliseconds per sample) with error bars across 10 seeds of Resnet-50 on ImageNet dataset with NVIDIA RTX A5000. Our Density-Softmax achieves almost the same weight and inference speed with a single Deterministic ERM model, as a result, outperforming other baselines in computational efficiency.

C.3.3. CALIBRATION DETAILS

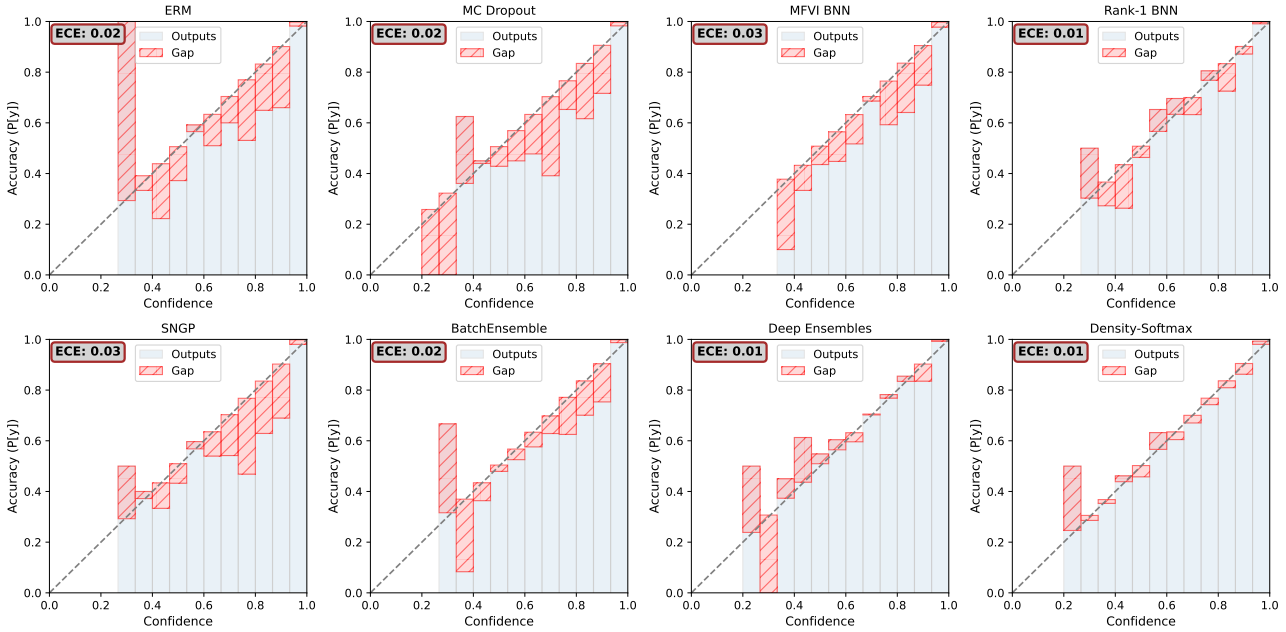

Figure 13. Reliability diagram of Density-Softmax versus different approaches, trained on CIFAR-10, test on IID CIFAR-10. Density-Softmax has a competitive calibration result with SOTA methods.

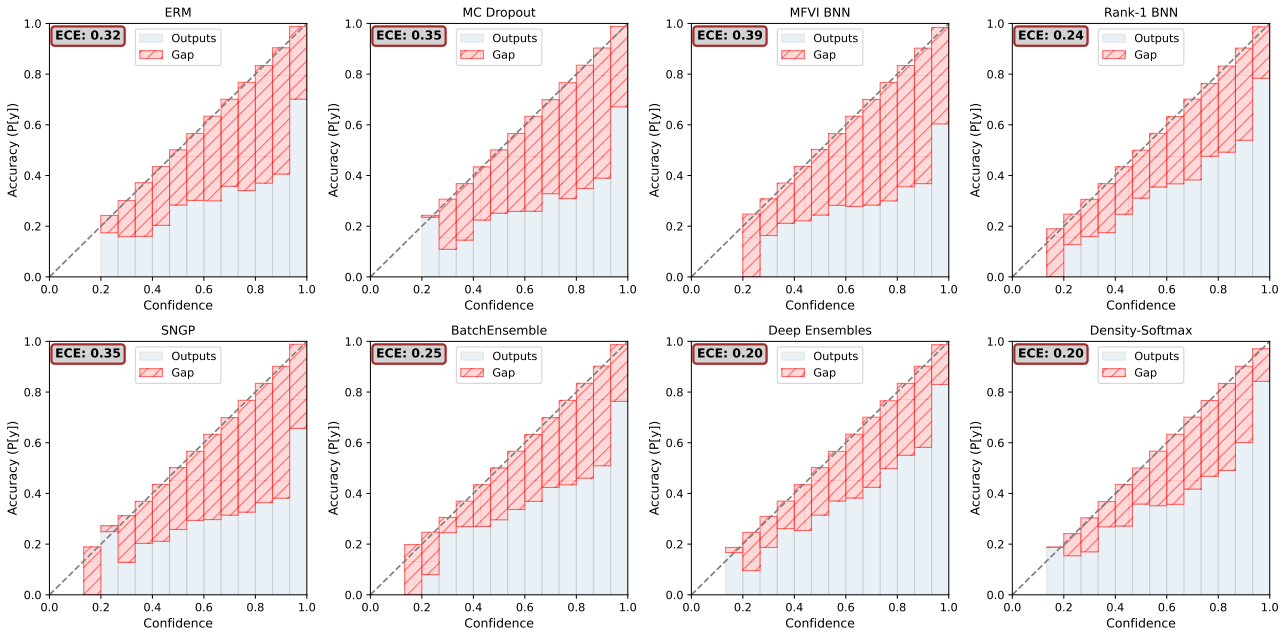

Figure 14. Reliability diagram of Density-Softmax versus different approaches, trained on CIFAR-10, test on OOD CIFAR-10-C set with "frosted glass blur" skew and "3" intensity. Density-Softmax has a competitive calibration result with SOTA methods.

To understand how models calibrate in more detail, we visualize the reliability diagrams to test the model's confidence across IID and OOD settings. For IID setting in CIFAR-10, Figure 13 illustrates our Density-Softmax is one of the best-calibrated models with a low ECE. On the one hand, compared to Deterministic ERM, MC Dropout, BatchEnsemble, and Deep

Ensemble, our model is less under-confidence than them in the prediction that has lower than about 0.4 confidence. On the other hand, compared to Deterministic ERM, MC Dropout, MFVI BNN, SNGP, and BatchEnsemble, our model is less over-confident than them in the prediction that has higher than about 0.4 confidence. As a result, accompanying Rank-1 BNN and Deep Ensembles, our model achieves the best calibration performance on IID data.

More importantly, we find that Density-Softmax is calibrated better than other methods on OOD data in Figure 14 and Figure 15. In particular, Figure 14 shows our model and Deep Ensembles achieves the lowest ECE and less over-confident than others in a particular CIFAR-10-C test set. Similarly, in real-world distributional shifts CIFAR-10.1 (v6), our model even achieves the lowest ECE with 0.01, outperforms the SOTA Deep Ensembles. These results once again confirm the hypothesis that our model is one of the best reliable models and especially robust under distributional shifts.

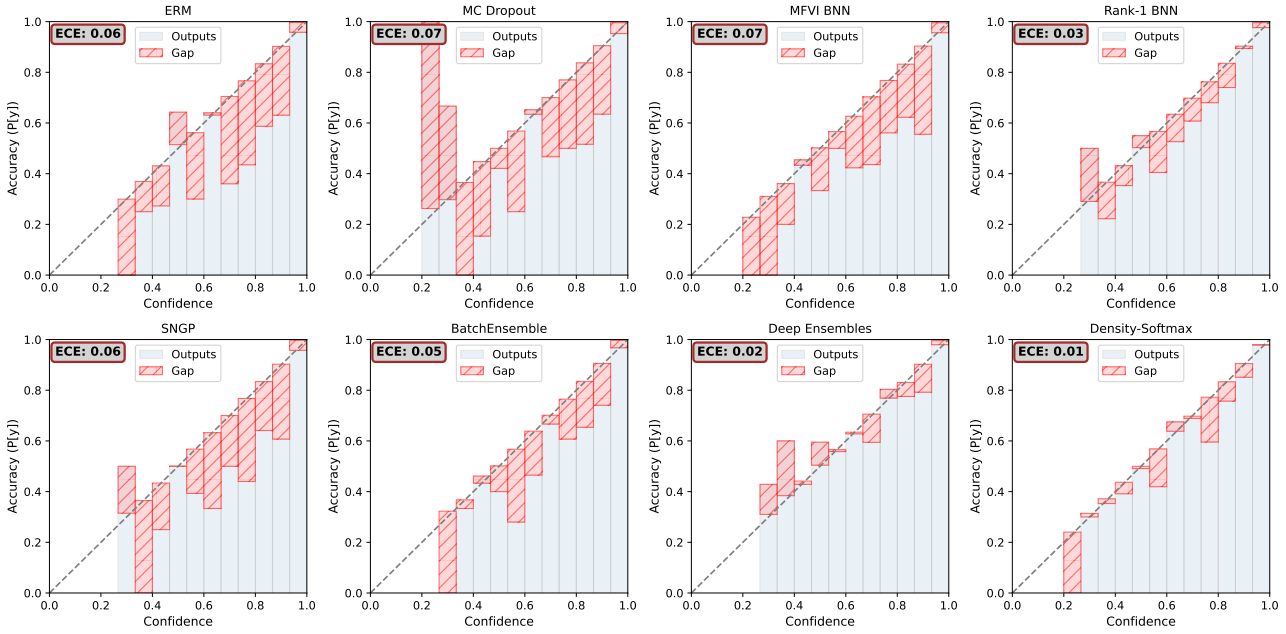

Figure 15. Reliability diagram of Density-Softmax versus different approaches, trained on CIFAR-10, test on real-world shifted OOD CIFAR-10.1 (v6). Density-Softmax is better-calibrated than other methods.

Miss-classified Expected Calibration Error. To evaluate the calibration quality in more detail, we continue to make a comparison in terms of Miss-classified ECE (Chen et al., 2022). This measurement is a specific case of ECE in Eq. 8. It is different by covering only the miss-classified samples. In this case, the lower mECE, the more honest of show uncertainty if the model makes wrong predictions. Fig. 16 illustrates the box plots of mECE across shift intensities. It confirms that Density-Softmax achieves the best performance with the lowest mECE, showing the ability to say "I don't know" before it makes the wrong predictions.

C.3.4. Predictive Entropy Details

Fig. 4 (a) has shown our trained model achieves the highest entropy value with a high density. Since this is the semantic shift, the highest entropy value indicates that our model is one of the best OOD detection models. Yet, this is only a necessary condition for a high-quality uncertainty estimation model because a pessimistic model could also achieve this performance. Therefore, to prove that Density-Softmax is not always under-confidence, we plot Fig. 17. We observe that Density-Softmax has a low predictive entropy with a high density on IID testing data, proving that our model is not under-confidence on IID data. Combined with the under-confidence on OOD data results, these show our Density-Softmax is a reliable model in terms of uncertainty estimation.

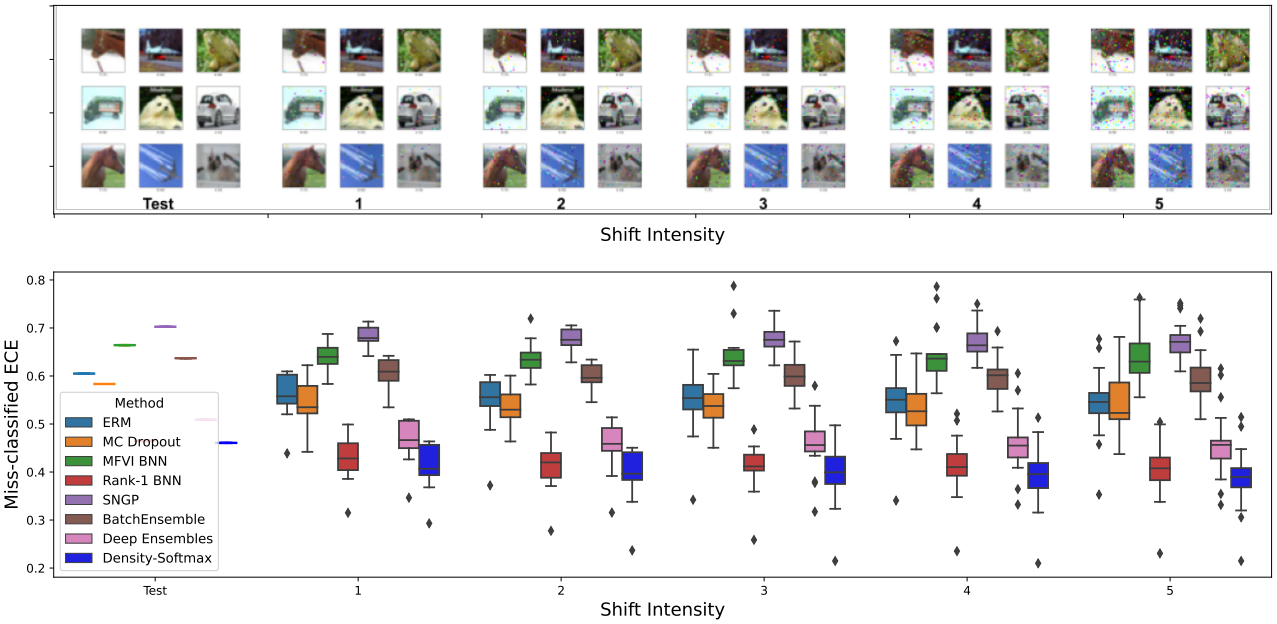

Figure 16. A corruption example by shift intensities and comparison under the distributional shift of miss-classified ECE under all types of corruptions in CIFAR-100-C (setting is similar to Figure 10). Our Density-Softmax achieves the lowest miss-classified ECE with low variance across different shift intensities.

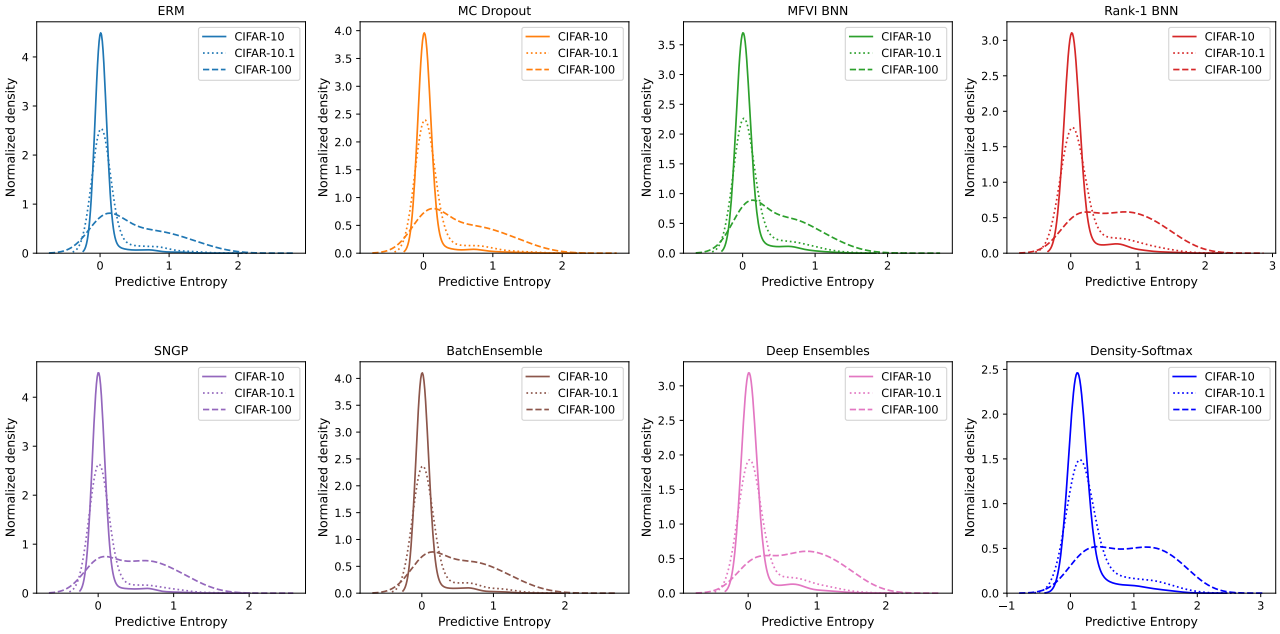

Figure 17. Histogram (bandwidth $= 0.5$) with density plot details from Figure 4 (a) of predictive entropy for each method on IID testing data CIFAR-10 (solid lines), covariate shift with OOD CIFAR-10.1 (v6) (dotted lines), and semantic shift with completely different OOD CIFAR-100 (dashed lines). Our Density-Softmax has a low predictive entropy value on IID while achieves the highest entropy value on OOD data.

Table 6. Condition dataset, hyper-parameters, and their default values in our experiments. Settings are inherited from Liu et al. (2020a) for the toy dataset and from Nado et al. (2021) for CIFAR-10-100 and ImageNet. Note that we always use the same hyper-parameters as the Deterministic ERM for a fair comparison.

Conditions	Hyper-parameters	Default value
Toy dataset	backbone	ResFFN-12-128 (Liu et al., 2020a)
	epochs	100
	batch size	128
	optimizer	Adam (Kingma & Ba, 2015)
	learning rate	1e-4
	density estimation epochs (Flows)	300
	density optimizer (Flows)	Adam (Kingma & Ba, 2015)
	density learning rate (Flows)	1e-4
	re-optimize classifier epochs	1
	gradient-penalty coefficient	1e-2
CIFAR-10-100	backbone	Wide Resnet-28-10 (Zagoruyko & Komodakis, 2016)
	epochs	200
	checkpoint interval	25
	batch size	64
	optimizer	SGD(momentum = 0.9, nesterov = True)
	learning rate	0.05
	lr decay epochs	[60, 120, 160]
	lr decay ratio	0.2
	L2 regularization coefficient	2e-4
	scale range	-[0.55-0.4, 0.4-0.3]
	density estimation epochs	50
	density optimizer	Adam (Kingma & Ba, 2015)
	density learning rate	1e-4
	re-optimize classifier epochs	10
	gradient-penalty coefficient	1e-4, 1e-5 (CIFAR-10, CIFAR-100)
ImageNet	backbone	Resnet-50 (He et al., 2016)
	epochs	90
	checkpoint interval	25
	batch size	64
	optimizer	SGD(momentum = 0.9, nesterov = True)
	learning rate	0.05
	lr decay epochs	[30, 60, 80]
	lr decay ratio	0.1
	L2 regularization coefficient	1e-4
	scale range	-[0.4, 0.3]
	density estimation epochs	10
	density optimizer	Adam (Kingma & Ba, 2015)
	density learning rate	1e-4
	re-optimize classifier epochs	2
	gradient-penalty coefficient	1e-1

Table 7. Two Coupling structures-(a) and (b) for Normalizing-Flows (Dinh et al., 2017; Papamakarios et al., 2021) on the Toy, CIFAR-10, CIFAR-100, and ImageNet. Input: $Z \in \mathbb{R}^{d_z}$, where $d_z = 128$ for ResFFN-12-128, $d_z = 640$ for Wide Resnet-28-10, and $d_z = 2048$ for Resnet-50.

(a) S_{θ_S}
Input: $Z \in \mathbb{R}^{d_z}$
Dense (units = 16, regularizers l2 = 0.01, ReLU)
Dense (units = 16, regularizers l2 = 0.01, ReLU)
Dense (units = 16, regularizers l2 = 0.01, ReLU)
Dense (units = 16, regularizers l2 = 0.01, ReLU)
Dense (units = 16, regularizers l2 = 0.01, Tanh)

(b) T_{θ_T}
Input: $Z \in \mathbb{R}^{d_z}$
Dense (units = 16, regularizers l2 = 0.01, ReLU)
Dense (units = 16, regularizers l2 = 0.01, ReLU)
Dense (units = 16, regularizers l2 = 0.01, ReLU)
Dense (units = 16, regularizers l2 = 0.01, ReLU)
Dense (units = 16, regularizers l2 = 0.01, Linear)

Table 8. Detailed table of Tab. 2.

Method	NLL(↓)	Acc(↑)	ECE(↓)	cNLL(↓)	cAcc(↑)	cECE(↓)	oNLL(↓)	oAcc(↑)	oECE(↓)	#Params(↓)	Latency(↓)
Deterministic ERM	0.159	96.0	0.023	1.05	76.1	0.153	0.40	89.9	0.064	**36.50M**	**518.12**
MC Dropout	0.145	96.1	0.019	1.27	70.0	0.167	0.39	89.9	0.058	36.50M	4,319.01
MFVI BNN	0.211	94.7	0.029	1.46	71.3	0.181	0.49	88.1	0.070	72.96M	809.01
Rank-1 BNN	0.128	96.3	**0.008**	0.84	76.7	0.080	0.32	90.4	0.033	36.65M	1,427.67
Posterior Net	0.360	93.1	0.112	1.06	75.2	0.139	0.42	87.9	0.053	36.60M	1,162.48
Heteroscedastic	0.156	96.0	0.023	1.05	76.1	0.154	0.38	90.1	0.056	36.54M	560.43
SNGP	0.134	96.0	0.007	0.74	78.5	0.078	0.43	89.7	0.064	37.50M	916.26
MIMO	0.123	96.4	0.010	0.93	76.6	0.112	0.35	90.1	0.037	36.51M	701.66
DUQ	0.239	94.7	0.034	1.35	71.6	0.183	0.49	87.9	0.068	40.61M	1,013.50
DDU (w/o TS)	0.159	96.0	0.024	1.06	76.0	0.153	0.39	89.8	0.063	37.60M	954.31
DUE	0.145	95.6	0.007	0.84	77.8	0.079	0.46	89.2	0.066	37.50M	916.26
NatPN	0.242	92.8	0.041	0.89	73.9	0.121	0.46	86.3	0.049	36.58M	601.35
BatchEnsemble	0.136	96.3	0.018	0.97	77.8	0.124	0.35	90.6	0.048	36.58M	1,498.01
Deep Ensembles	**0.114**	**96.6**	0.010	0.81	77.9	0.087	0.28	**92.2**	0.025	145.99M	1,520.34
Density-Softmax	0.137	96.0	0.010	**0.68**	**79.2**	**0.060**	**0.26**	91.6	**0.016**	36.58M	**520.53**

Table 9. Detailed table of Tab. 3.

Method	NLL(↓)	Acc(↑)	ECE(↓)	cNLL(↓)	cAcc(↑)	cECE(↓)	AUPR-S(↑)	AUPR-C(↑)	#Params(↓)	Latency(↓)
Deterministic ERM	0.875	79.8	0.086	2.70	51.4	0.239	0.882	0.745	**36.55M**	**521.15**
MC Dropout	0.785	80.7	0.049	2.73	46.2	0.207	0.832	0.757	36.55M	4,339.03
MFVI BNN	0.944	77.8	0.097	3.18	48.2	0.271	0.882	0.748	73.07M	818.31
Rank-1 BNN	0.692	81.3	**0.018**	2.24	53.8	0.117	0.884	0.797	36.71M	1,448.90
Posterior Net	2.021	77.3	0.391	3.12	48.3	0.281	0.880	0.760	36.60M	11,243.84
Heteroscedastic	0.833	80.2	0.059	2.40	52.1	0.177	0.881	0.752	37.00M	568.17
SNGP	0.805	80.2	0.020	2.02	54.6	0.092	**0.923**	0.801	37.50M	926.99
MIMO	0.690	82.0	0.022	2.28	53.7	0.129	0.885	0.760	36.68M	718.11
DUQ	0.980	78.5	0.119	2.84	50.4	0.281	0.878	0.732	77.58M	1,034.66
DDU (w/o TS)	0.877	79.7	0.086	2.70	51.3	0.240	0.890	0.797	37.60M	959.25
DUE	0.902	79.1	0.038	2.32	53.5	0.127	0.897	0.787	37.50M	926.99
NatPN	1.249	76.9	0.091	2.97	48.0	0.265	0.875	0.768	36.64M	613.44
BatchEnsemble	0.690	81.9	0.027	2.56	53.1	0.149	0.870	0.757	36.63M	1,568.77
Deep Ensembles	**0.666**	**82.7**	0.021	2.27	54.1	0.138	0.888	0.780	146.22M	1,569.23
Density-Softmax	0.780	80.8	0.038	**1.96**	**54.7**	**0.089**	0.910	**0.804**	36.64M	**522.94**

Table 10. Detailed table of Tab. 4.

Method	NLL(↓)	Acc(↑)	ECE(↓)	cNLL(↓)	cAcc(↑)	cECE(↓)	#Params(↓)	Latency(↓)
Deterministic ERM	0.939	76.2	0.032	3.21	40.5	0.103	**25.61M**	**299.81**
MC Dropout	0.919	76.6	0.026	2.96	42.4	0.046	25.61M	601.15
Rank-1 BNN	0.886	77.3	0.017	2.95	42.9	0.054	26.35M	690.14
Heteroscedastic	0.898	77.5	0.033	3.20	42.4	0.111	58.39M	337.50
SNGP	0.931	76.1	**0.013**	3.03	41.1	0.045	26.60M	606.11
MIMO	0.887	77.5	0.037	3.03	43.3	0.106	27.67M	367.17
BatchEnsemble	0.922	76.8	0.037	3.09	41.9	0.089	25.82M	696.81
Deep Ensembles	**0.857**	**77.9**	0.017	2.82	**44.9**	0.047	102.44M	701.34
Density-Softmax	0.885	77.5	0.019	**2.81**	44.6	**0.042**	25.88M	**299.90**